Detailed Absorption, Reflectance, and UV Photoelectron Spectroscopic and Theoretical Studies of the Charge-Transfer Transitions of $CuCl_4^{2-}$: Correlation of the Square-Planar and the Tetrahedral Limits

Sylvie R. Desjardins,[1a] Kevin W. Penfield,[1a,b] Susan L. Cohen,[1a,b] Ronald L. Musselman,[1b,c] and Edward I. Solomon*[1a,b]

Contribution from the Department of Chemistry, Stanford University, Standford, California 94305, the Department of Chemistry, Massachusetts Institute of Technology, Cambridge, Massachusetts 02139, and the Department of Chemistry, Principia College, Elsah, Illinois 62028. *Received November 8, 1982*

Abstract: Low-temperature (7 K) polarized single-crystal absorption and room-temperature polarized specular reflectance spectra have been obtained of the chloride-to-copper charge-transfer region of the three known square-planar salts of $CuCl_4^{2-}$, bis(methadonium) tetrachlorocuprate(II), bis(*N*-methylphenethylammonium) tetrachlorocuprate(II), and bis(creatinium) tetrachlorocuprate(II) and of the tetragonal monomer, bis(ethylammonium) tetrachlorocuprate(II). These spectra show two intense, x-y polarized, x-y split transitions in the regions 26 000–28 000 and 37 000–39 000 cm^{-1}. These bands are assigned to the allowed $^2E_u \leftarrow {}^2B_{1g}$ ($4e_u(\pi) \rightarrow 3b_{1g}$) and $^2E_u \leftarrow {}^2B_{1g}$ ($3e_u(\sigma) \rightarrow 3b_{1g}$) transitions, respectively. In addition, a weaker band is observed between 22 000 and 25 000 cm^{-1} and has been assigned to the $^2A_{2g} \leftarrow {}^2B_{1g}$ ($1a_{2g}(nb) \rightarrow 3b_{1g}$) transition. These assignments are compared to the results of SCF-Xα-SW ground- and transition-state calculations; although the calculated transition energies are too low and there is overlap of the calculated d–d and charge-transfer manifolds of states (in contrast to the clean separations observed experimentally), the differences between the calculated energies of the three charge-transfer transitions agree well with those observed experimentally. The assignment is also supported by He(II) ultraviolet photoelectron spectroscopic data on single crystals of $(C_2H_5NH_3)_2CuCl_4$ and $(CH_3NH_3)_2CuCl_4$. In light of these assignments for the square planar (D_{4h}) $CuCl_4^{2-}$ ion, the charge-transfer spectrum of the flattened tetrahedral (D_{2d}) $CuCl_4^{2-}$ ion has been reassigned (the tetrahedral parentage of the excited state is indicated in parentheses): 22 700 cm^{-1} (sh), $^2A_2(^2T_1,nb) \leftarrow {}^2B_2(^2T_2)$; 24 730 cm^{-1}, $^2E(^2T_1,nb) \leftarrow {}^2B_2(^2T_2)$; 28 880 cm^{-1} (sh), $^2E(^2T_2,\pi) \leftarrow {}^2B_2(^2T_2)$; 33 480 cm^{-1}, $^2E(^2T_2,\sigma) \leftarrow {}^2B_2(^2T_2)$; 43 000 cm^{-1}, $^2A_1(^2A_1,\sigma) \leftarrow {}^2B_2(^2T_2)$. These assignments require all of the chloride π- and σ-derived charge-transfer transitions to contribute to the visible–ultraviolet absorption spectrum within a 20 000-cm^{-1} region. This spread in energy is supported by both SCF-Xα-SW ground- and transition-state calculations and UPS studies on single crystals of Cs_2CuCl_4. In addition, the lack of intensity of the group theoretically allowed $^2A_1 \leftarrow {}^2B_2$ ($3a_1(\pi) \rightarrow 5b_2$) transition in D_{2d} and the allowed $^2B_{2u} \leftarrow {}^2B_{1g}$ ($1b_{2u}(\pi) \rightarrow 3b_{1g}$) transition in D_{4h} is explained by a simple model for charge-transfer transition intensities. The contributions of many-electron reorganization effects to optical and UPS transitions are examined in a comparison of both experimental and theoretical data. The results indicate that, because of differences in electron–electron repulsion and orbital relaxation, one must be cautious in attempting to correlate UPS and optical transition energy differences. Finally, the factors that contribute to the differences between energies of related charge-transfer transitions in the D_{4h} and D_{2d} geometries are evaluated by using the experimental and theoretical results. It is concluded that while crystal-field effects are quite significant, shifting the energy of the $d_{x^2-y^2}$ orbital by ~5000 cm^{-1}, changes in ligand–ligand repulsion can be equally important (4000 cm^{-1} for the $^2A_{2g} \leftarrow {}^2B_{1g}$ ($1a_{2g}(nb) \rightarrow 3b_{1g}$) transition). Differences in many-electron reorganization effects and configuration interaction (due to changes in overlap) can also make major contributions to changes in transition energies.

Introduction

Considerable interest has been shown over the years in electronic theoretical and spectral studies of the $CuCl_4^{2-}$ complex because of the relative simplicity of its geometric and electronic structure.[2-5] This d^9, one-hole complex is found in a variety of geometries ranging from flattened tetrahedral (D_{2d}) to square planar (D_{4h}); several examples of this latter limit have recently been characterized.[6] Correlations of the ligand-field (d–d) transitions in these two geometries have been made possible through accurate spectral assignments. In the D_{2d} case the d–d transitions are electric dipole allowed; the polarized single-crystal spectral studies of Ferguson[3b] have generated the order $^2B_2(x^2-y^2)$ (ground state) < $^2E(xz, yz)$ < $^2B_1(xy)$ < $^2A_1(z^2)$ (see Figure 1).[7] Assignment of the square-planar limit has been more difficult, as this geometry possesses inversion symmetry, and the d–d transitions are therefore made allowed through vibronic coupling. However, Hitchman[4d] has recently studied the highly vibrationally structured d–d transitions in the bis(*N*-methylphenethylammonium) tetrachlorocuprate(II) complex and applied vibronic selection rules to determine the square-planar ordering: $^2B_{1g}(x^2-y^2)$ (ground state) < $^2B_2(xy)$ < $^2E_g(xz, yz)$ < $^2A_{1g}(z^2)$. The observed shifts, between these two geometries, in the energies of the d–d transitions have been explained through ligand-field theory,[5a-f] one-electron molecular orbital bonding theory,[5g-i] and, more recently, through many-electron bonding calculations.[5j-m]

These ligand-field spectral studies of small molecule inorganic copper complexes have proved to be invaluable in elucidating the

* To whom all correspondence should be addressed at Stanford University.

(1) (a) Massachusetts Institute of Technology; (b) Stanford University; (c) Principia College.

(2) (a) Smith, D. W. *Coord. Chem. Rev.* **1976**, *21*, 93. (b) Smith, D. W. *Struct. Bonding (Berlin)* **1972**, *12*, 49.

(3) (a) Furlani, C.; Morpurgo, G. *Theor. Chim. Acta* **1963**, *1*, 102. (b) Ferguson, J. *J. Chem. Phys.* **1964**, *40*, 3406. (c) Sharnoff, M.; Reimann, C. W. *Ibid.* **1967**, *46*, 2634. (d) Bird, B. D.; Day, P. *J. Chem. Soc., Chem. Commun.* **1967**, 741. (e) Bird, B. D.; Day, P. *J. Chem. Phys.* **1968**, *49*, 392. (f) Bird, B. D.; Briat, B.; Day, P.; Rivoal, J. C. *Symp. Faraday Soc.* **1969**, *3*, 70. (g) Rivoal, J. C.; Briat, B. *Mol. Phys.* **1974**, *27*, 1081.

(4) (a) Cassidy, P.; Hitchman, M. A. *J. Chem. Soc., Chem. Commun.* **1975**, 837. (b) Cassidy, P.; Hitchman, M. A. *Inorg. Chem.* **1977**, *16*, 1568. (c) Hitchman, M. A. *J. Chem. Soc., Chem. Commun.* **1979**, 973. (d) Hitchman, M. A.; Cassidy, P. J. *Inorg. Chem.* **1979**, *18*, 1745. (e) Hitchman, M. A.; Cassidy, P. J. *Ibid.* **1978**, *17*, 1682. (f) Heygster, G.; Kleeman, W. *Physica B+C (Amsterdam)* **1977**, *89B+C*, 165.

(5) (a) Day, P. *Proc. Chem. Soc.* **1964**, 18. (b) Hatfield, W. E.; Piper, T. S. *Inorg. Chem.* **1964**, *3*, 841. (c) Smith, D. W. *J. Chem. Soc. A* **1969**, 2529. (d) Smith, D. W. *Ibid.* **1970**, 2900. (e) Smith, D. W. *Inorg. Chim. Acta* **1977**, *22*, 107. (f) Solomon, E. I.; Hare, J. W.; Dooley, D. M.; Dawson, J. H.; Stephens, P. J.; Gray, H. B. *J. Am. Chem. Soc.* **1980**, *102*, 168. (g) Lohr, L. L., Jr.; Lipscomb, W. N. *Inorg. Chem.* **1963**, *2*, 911. (h) Day, P.; Jorgensen, C. K. *J. Chem. Soc.* **1964**, 6226. (i) Ros, P.; Schuit, G. C. A. *Theor. Chim. Acta* **1966**, *4*, 1. (j) Johnson, K. H.; Wahlgren, U. *Int. J. Quantum. Chem., Quantum Chem. Symp.* **1972**, *6*, 243. (k) Demuynck, J.; Veillard, A.; Wahlgren, U. *J. Am. Chem. Soc.* **1973**, *95*, 5563. (l) Correa de Mello, P.; Hehenberger, M.; Larsson, S.; Zerner, M. *Ibid.* **1980**, *102*, 1278. (m) Barker, M.; Clark, J. D.; Hinchcliffe, A. *J. Chem. Soc., Faraday Trans. 2* **1978**, *74*, 681.

0002-7863/83/1505-4590$01.50/0

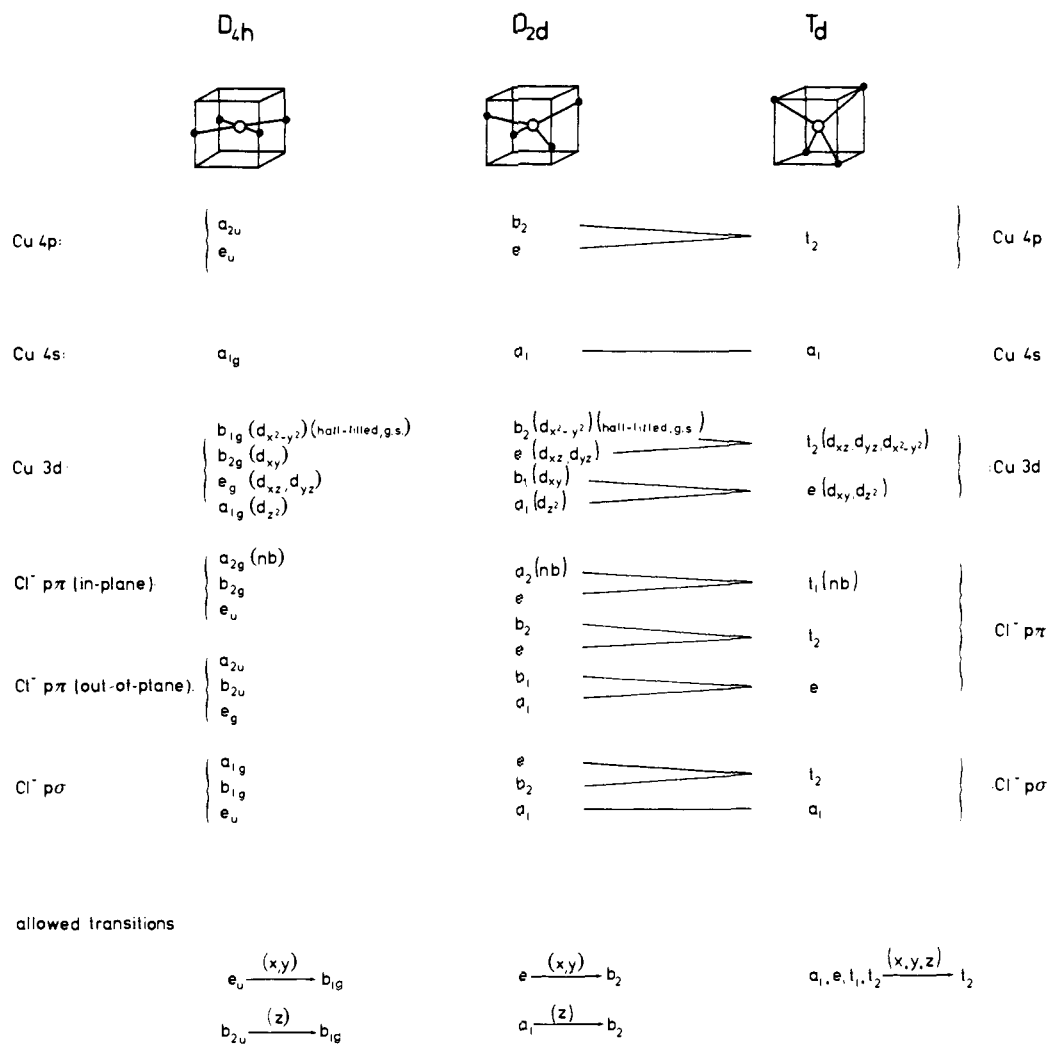

Figure 1. Molecular orbitals in D_{4h}, D_{2d}, and T_d symmetry. Top: The geometries of $CuCl_4^{2-}$ ions with each of these three symmetries are indicated. Center: The symmetries of the molecular orbitals composed of the Cu and Cl valence orbitals; nb indicates the nonbonding orbitals. The atomic orbitals from which the bracketed MO's are generated are given on the side columns. The correlation of orbitals in D_{2d} and their parent orbitals in T_d is indicated by solid lines between the corresponding orbitals. Bottom: The dipole-allowed transitions and their polarizations.

spectroscopically effective active site[5f,8] of the blue copper proteins prior to their crystallographic structure determination.[9] The observation of d–d transitions in the near-infrared region in the spectra of these proteins (in comparison with ligand-field calculations similar to those mentioned above) required that the protein site be close to tetrahedral.[5f,8] The visible/near-ultraviolet absorption spectra of these copper proteins are dominated by ligand-to-copper charge-transfer transitions. However, most studies modeling these active sites[10] have involved tetragonal (square planar) complexes. Thus, attempts at correlating the charge-transfer transitions of these models with those of the protein sites have raised a number of important questions concerning the factors involved in correlating charge-transfer transitions between the square-planar and tetrahedral geometries. A simple model that has been widely used assumes that due to the large decrease in crystal-field destabilization of the $d_{x^2-y^2}$ orbital upon distortion from square planar to tetrahedral, the energy of all ligand to Cu $d_{x^2-y^2}$ charge-transfer transitions will decrease in energy by the same amount as the $d_{x^2-y^2}$ orbital. Here the energy of the ligand orbitals are presumed to be unaffected by the geometric distortion. Further, in recent attempts to obtain a detailed assignment of the blue copper protein charge-transfer spectrum, a one-to-one quantitative comparison between the related ligand ultraviolet photoelectron spectrum (UPS) and the protein optical absorption spectra has been assumed. This ignores the effects of changes in electron–electron repulsion induced upon optical or UPS excitation and orbital relaxation effects are not considered. Although useful in obtaining a qualitative understanding of charge-transfer transition energies, both of these simple approximations can be misleading, and thus other factors must be considered. Due to their high symmetry and the variety of well-defined geometries available, the tetrachlorocuprate system provides an ideal electronic structural model for the quantitative evaluation of these factors that contribute to the charge-transfer transition energies.

The charge-transfer region of the D_{2d} Cs_2CuCl_4 complex has been the subject of several polarized single-crystal spectral studies.[3b,c] The intense transitions in this region have been made accessible to spectral study by dilution of the $CuCl_4^{2-}$ complex into the isomorphous, transparent Cs_2ZnCl_4 lattice[3c] and by epitaxial deposition of a thin layer of Cs_2CuCl_4 on a pure Cs_2ZnCl_4

(6) (a) Harlow, R. L.; Wells, W. J., III; Watt, G. W.; Simonsen, S. H. *Inorg. Chem.* **1974**, *13*, 2106. (b) Nelson, H. C.; Simonsen, S. H.; Watt, G. W. *J. Chem. Soc., Chem. Commun.* **1979**, 632. (c) Harlow, R., private communication. (d) Udupa, M. R.; Krebs, B. *Inorg. Chim. Acta* **1979**, *33*, 241.

(7) Note that here we use an x,y coordinate system as defined in ref 8 that is rotated 45° relative to the usual D_{2d} axes but more easily allows correlation to the $d_{x^2-y^2}$ ground-state orbital in the square-planar limit.

(8) Solomon, E. I.; Hare, J. W.; Gray, H. B. *Proc. Natl. Acad. Sci. U.S.A.* **1976**, *73*, 1389.

(9) (a) Colman, P. J.; Freeman, H. C.; Guss, J. M.; Murata, M.; Norris, V. A.; Ramshaw, J. A. M.; Venkatappa, M. P. *Nature (London)* **1978**, *272*, 319. (b) Adman, E. T.; Stenkamp, R. E.; Sieker, L. C.; Jensen, L. H. *J. Mol. Biol.* **1978**, *123*, 35. (c) Adman, E. T.; Jensen, L. H. *Isr. J. Chem.* **1981**, *21*, 8.

(10) (a) Gray, H. B.; Solomon, E. I. In "Copper Proteins"; Spiro, T. G., Ed.; Wiley-Interscience: New York, 1981; p 1. (b) Solomon, E. I.; Penfield, K. W.; Wilcox, D. E. *Struct. Bonding (Berlin)* **1983**, *53*, 1.

substrate.[3b] In addition, since the $CuCl_4^{2-}$ complex has the D_{2d} geometry in solution, these single-crystal studies were complemented by a series of low-temperature absorption[3e,g] and room-[3f] and low-temperature[3g] magnetic circular dichroism studies on glasses and films. On the basis of these studies, the present assignment of the charge-transfer spectrum of D_{2d} $CuCl_4^{2-}$ attributes all of the bands between 20 000 and 45 000 cm^{-1} to Cl $p(\pi) \rightarrow$ Cu charge-transfer transitions (see Figure 1).[3g] Prior to the present work, no analogous single-crystal polarized optical charge-transfer studies had been pursued on the D_{4h} $CuCl_4^{2-}$ since an isomorphous, transparent lattice does not presently exist. However, polarized absorption studies of the low-energy part of the charge-transfer spectrum of the square-planar methadonium salt of $CuCl_4^{2-}$ have been possible because the large size of the cation provides a significant dilution factor relative to the other D_{4h} $CuCl_4^{2-}$ unit cells. The higher energy transitions in several D_{4h} $CuCl_4^{2-}$ salts have been studied by polarized single-crystal reflectance spectroscopy. The spectra obtained through this technique can be related to polarized absorption spectra through the Kramers–Kronig transformation. The small structural variations that are present among the different salts provide perturbations to aid in spectral assignment.

The studies reported here have enabled a complete assignment to be made of the charge-transfer region of D_{4h} $CuCl_4^{2-}$ (between 20 000 and 40 000 cm^{-1}) in terms of all of the allowed π and σ charge-transfer transitions. The correlation of these results to the D_{2d} case requires a revision of the assignment of the D_{2d} charge-transfer spectrum. This revision is supported by the results of single-crystal ultraviolet photoelectron spectroscopic (UPS) studies and optical and photoionization transition state SCF-Xα-SW calculations. The comparison of UPS and optical results also provides insight into the differing contributions of many-electron effects in these two techniques. Finally, the factors involved in the changes in energy and intensity of the charge-transfer transitions upon distortion of $CuCl_4^{2-}$ from D_{4h} to D_{2d} are discussed in light of these experimental spectral assignments.

Experimental Section

Four different $CuCl_4^{2-}$ salts were studied by linearly polarized spectroscopy. Their crystals are all biaxial, belonging to the orthorhombic or monoclinic systems. In obtaining linearly polarized spectra of anisotropic crystals, care must be taken to prevent the incident plane-polarized light from becoming elliptically polarized and thereby causing mixing of the polarized spectra. This problem is avoided by propagating the incident polarized light such that the plane defined by the E vector and the direction of propagation contains one of the *principal*[11] axes of the crystals. In orthorhombic crystals, the principal axes are required by symmetry to be parallel to the three mutually perpendicular 2-fold axes of the unit cell. For monoclinic crystals, one of the principal axes is required to be parallel to the unique 2-fold axis; the only restriction on the other two principal axes is that they must be perpendicular to this 2-fold axis and each other. Hence, the polarization directions are fixed when the crystal face under examination contains the 2-fold b axis (as in the case of bis(methadonium) tetrachlorocuprate(II) and bis(creatininium) tetrachlorocuprate(II) below): the planes of polarization of the incident light are simply aligned parallel and perpendicular to the b axis. However, when the face of interest is perpendicular to the b axis (as in the case of bis(N-methylphenethylammonium) tetrachlorocuprate(II) below), the lack of crystallographic symmetry requirements in this plane *may* cause the principal axes to change their orientation as temperature and wavelength are varied. However, even for the {010} face of bis(N-methylphenethylammonium) tetrachlorocuprate(II), these directions were not observed to vary as a function of either wavelength or temperature.[4d]

Large, well-formed needles of bis(N-methylphenethylammonium) tetrachlorocuprate(II) (hereafter referred to as $(N\text{-mpH})_2CuCl_4$) were obtained by slow diffusion of ether into a stoichiometric solution of N-methylphenethylamine hydrochloride and anhydrous $CuCl_2$ in acetone.[6a] The predominant faces of these hexagonal needles were {010}, {021}, and {02$\bar{1}$}. These monoclinic crystals belong to the space group $P2_1/c$ and contain two molecules per unit cell. The site symmetry of the copper atom is C_i, while the effective symmetry of the $CuCl_4^{2-}$ is D_{2h}, being distorted from D_{4h} by a small difference in the Cu–Cl bond lengths. There is no axial ligation. Polarized reflectance spectra were obtained on the {010} face; the extinction directions on this face are oriented at +6 and −84° to the a axis, the plus sign corresponding to a rotation of the electric vector into the quadrant containing an obtuse angle. Polarized spectra were not obtained on the other two faces, as each of these is almost normal to an optic axis, causing complete mixing of the polarizations. Defining a molecular coordinate system with $\vec{x}$ along the shorter Cu–Cl bond, $\vec{y}$ orthogonal to $\vec{x}$ and in the general direction of the longer Cu–Cl bond, and $\vec{z}$ orthogonal to both $\vec{x}$ and $\vec{y}$, the following relationships hold:

$$I_{+6^\circ \text{ to } a \text{ axis}} = 0.610I_x + 0.001I_y + 0.389I_z \quad (1)$$

$$I_{-84^\circ \text{ to } a \text{ axis}} = 0.201I_x + 0.519I_y + 0.281I_z \quad (2)$$

Bis(methadonium) tetrachlorocuprate(II) crystals (hereafter referred to as $(metH)_2CuCl_4$) were prepared by Dr. Harold C. Nelson by the addition of stoichiometric quantities of methadone hydrochloride and $CuCl_2$ to acetone–ether and the subsequent slow evaporation of this solution.[6b] These monoclinic crystals (space group $P2_1/c$; two molecules per unit cell) were obtained as diamond-shaped plates. Precession photographs subsequently identified the predominant face of these plates as {100}. The symmetry of the copper site is C_i, while the square planar $CuCl_4^{2-}$ unit again possesses a D_{2h} geometry, with two slightly inequivalent Cu–Cl bond lengths. After these crystals were polished to the smallest possible thickness, polarized absorption spectra were obtained of the {100} face and the $a'b$ face, where $a' \perp c$. In both cases, the incident light was polarized parallel and perpendicular to b. With the same molecular coordinate system described above for the $(N\text{-mpH})_2CuCl_4$ salt, the following equations are obtained for the $(metH)_2CuCl_4$ case:[6c]

$$I_{a'} = 0.166I_x + 0.773I_y + 0.062I_z \quad (3)$$

$$I_b = 0.715I_x + 0.217I_y + 0.068I_z \quad (4)$$

$$I_c = 0.119I_x + 0.011I_y + 0.870I_z \quad (5)$$

Bis(creatinium) tetrachlorocuprate(II) crystals (hereafter referred to as $(creat)_2CuCl_4$) were prepared by the method of Udupa and Krebs.[6d] These crystals grow as well-formed flat plates; precession photographs again were used to identify the predominant faces as {100}, in agreement with the findings of Hitchman,[4c] who studied the d–d spectrum of this salt. They are somewhat hygroscopic and belong to the $P2_1/c$ space group, with two molecules per unit cell, C_i site symmetry at the copper atom, and a $CuCl_4^{2-}$ unit with D_{2h} symmetry, again being distorted from D_{4h} by a small difference in the lengths of the Cu–Cl bonds. Polarized absorption spectra were taken with light propagating normal to very thin {100} slices, while specular reflectance spectra were taken of natural {100} and {001} faces (polarized parallel and perpendicular to b in all cases). Defining the usual molecular coordinate system, the following equations are obtained for $(creat)_2CuCl_4$:

$$I_a = 0.022I_x + 0.661I_y + 0.317I_z \quad (6)$$

$$I_b = 0.978I_x + 0.014I_y + 0.008I_z \quad (7)$$

$$I_c = 0.004I_x + 0.038I_y + 0.958I_z \quad (8)$$

Single crystals of $(C_2H_5NH_3)_2CuCl_4$[12a] and $(CH_3NH_3)_2CuCl_4$[12b,c] were grown by the slow evaporation of a stoichiometric mixture of the amine hydrochloride (obtained commercially) and $CuCl_2 \cdot 2H_2O$ in methanol. The mica-like $(C_2H_5NH_3)_2CuCl_4$ crystals grow with the {100} faces predominating. These crystals belong to the orthorhombic space group $Pbca$, with four molecules per unit cell and C_i symmetry at the copper site. Although a complete crystal structure has not been performed on the $(CH_3NH_3)_2CuCl_4$, it is believed to have a similar structure.[12b,c] The $CuCl_4^{2-}$ units, which have D_{4h} symmetry, form an infinite framework, with two of the equatorial chloride ligands of one unit acting as the distant axial ligands of adjacent units [$Cu\text{–}Cl_{eq}$ = 2.28 Å; $Cu\text{–}Cl_{ax}$ = 2.98 Å]. Defining a molecular coordinate system with $\vec{x}$ and $\vec{y}$ pointing along the two short Cu–Cl bonds (which have equal lengths, within experimental error) and $\vec{z}$ along the long Cu–Cl bond, the following equations are obtained:

(11) (a) Born, M.; Wolf, E. "Principles of Optics"; Pergamon Press: New York, 1965; p 708. (b) Pancharatnam, S. *Proc. Indian Acad. Sci., Sect. A* **1955**, *42*, 86. (c) Martin, D. S.; Newman, R. A.; Fanwick, P. E. *Inorg. Chem.* **1979**, *18*, 2511.

(12) (a) Steadman, J. P.; Willett, R. D. *Inorg. Chim. Acta* **1970**, *4*, 367. (b) Arend, H.; Huber, W.; Mischgofsky, F. H.; Richter-van Leeuwen, G. K. *J. Cryst. Growth* **1978**, *43*, 213. (c) Willett, R. D. *J. Chem. Phys.* **1964**, *41*, 2243.

$$I_a = 0.994I_{xy} + 0.006I_z \quad (9)$$

$$I_b = 0.489I_{xy} + 0.511I_z \quad (10)$$

$$I_c = 0.517I_{xy} + 0.483I_z \quad (11)$$

Hence the absorption spectra obtained with light incident on the {100} faces of thinly polished natural crystals were unpolarized.

Single crystals of Cs_2CuCl_4 were grown by the slow evaporation of an aqueous solution of CsCl and $CuCl_2 \cdot 2H_2O$ in a 3.5:1 ratio.[3c] These orthorhombic crystals[13] belong to the space group *Pnam* with four molecules per unit cell and C_i symmetry at the copper site. The $CuCl_4^{2-}$ units have a C_s distorted D_{2d} effective symmetry.

Low-temperature linearly polarized absorption spectra were obtained by using a McPherson RS-10 double-beam spectrometer and Janis Super Vari-Temp helium Dewar as previously described.[14] Polarization of the light beam was accomplished by using a matched pair of Glan-Taylor calcite prism polarizers that have a spectral range of 2140 Å–2.3 μm.

Polarized specular reflectance spectra were obtained on an instrument based upon a design by Anex.[15] The core of the instrument is a polarizing microscope fitted with reflecting optics to eliminate continual refocusing through a spectral scan. Examples studied had naturally grown faces that, although usually irregular in the planarity and thus reflectivity, were highly reflective in small regions of uniform planarity. The microscope optics (20×) allowed inspection for and limiting of the spectrum to good regions as small as 20 μm in diameter. The sample was illuminated by either a quartz–halogen lamp or a high-pressure deuterium lamp through a Beckman DU monochromator and a Glan-Thompson polarizing prism. Signal detection was with an RCA 4840 photomultiplier and a PAR 186-A lock-in amplifier. Data were interfaced to an HP 3000-III for collection and processing. Low temperatures were achieved through an Air Products and Chemicals' Cryo-Tip Joule Thompson refrigerator, allowing continuously adjustable temperatures from ambient to liquid nitrogen.

Absolute reflectivities were determined by referencing the sample signal to a MgF_2-coated aluminum reference mirror, then correcting for Al reflectivity.[16] Three to five spectra were averaged for each sample. Absorption parameters were obtained through Kramers–Kronig transformation[17] of the reflection data. This technique is based upon the Fresnel relationship between absorptivity coefficient (k), reflectivity (r), and phase change upon reflection (θ):

$$k = \frac{-2r \sin \theta}{1 + r^2 - 2r \cos \theta}$$

in which the phase change at frequency ω is related to reflectivity through the Kramers–Kronig equation:

$$\theta(\omega) = \frac{2\omega}{\pi} \int_0^\infty \frac{\ln r(\omega') - \ln r(\omega)}{\omega'^2 - \omega^2} \, d\omega'$$

where reflectivities at all energies contribute to values for θ. This expression needs to be divided into three regions since experimental data are not available at extreme high and low energies. The low-energy portion generally does not have transitions that affect the phase change, so the reflectivity is taken as constant from the lowest energy experimental values. The high-energy portion generally does have transitions in the vacuum ultraviolet that affect the phase of the reflected light in the experimentally measured region. These transitions are represented by a reflection band that decreases to zero at higher energies. The height of the tail out to infinity affects the value of the minima in the transformed spectra in the experimental region and is adjusted to give zero absorbance at appropriate energies in the experimental region. Such adjustments do not affect transition energies of absorption bands.

Self-consistent field Xα scattered wave (SCF-Xα-SW) calculations[18] were performed by using programs provided by Professor Keith Johnson of the MIT Materials Science Department. Through this numerical technique, one-electron wave functions and energy eigenvalues can be calculated for molecules and ions. In order to take relaxation into account in the calculation of the energies of electronic transitions, Slater's transition-state concept[18a] is used. In this method, an intermediate state is generated by reducing the occupancy of the orbital from which the transition originates by 0.5 electron and increasing the occupancy of the final orbital by 0.5 electron. The potential thereby produced must then be converged; the resultant energy difference between the two half-occupied orbitals is equal to the transition energy. In the calculation of ionization potentials, 0.5 electron is removed from the orbital of interest and the potential is reconverged, retaining the original charge on the Watson (outer) sphere. The ionization potential is then equal to the energy eigenfunction of the partially occupied orbital.

For both the D_{4h} and D_{2d} geometries, spin-restricted calculations were performed for the ground state, all of the d–d and Cl 3p to Cu charge-transfer transition states, some transition states involving low-lying Rydberg states, and all of the ionization transition states from valence levels. Spin-polarized calculations were also performed on the ground states in both geometries; the orbital ordering and energies derived for these calculations differed very little from the spin-restricted results. In the calculations of the D_{4h} ion, the average (2.265 Å) of the Cu–Cl bond lengths found in the $(N\text{-mpH})_2CuCl_4$ salt[6a] were used, with atomic radii of 1.269 Å for Cu and 1.306 Å for Cl. For the D_{2d} ion, the structural data for Cs_2CuCl_4 were used:[13] the averages of all Cu–Cl bond lengths (2.230 Å), the two small Cl–Cu–Cl angles (100.7°), and the two large Cl–Cu–Cl angles (129.2°). The atomic radii were 1.249 Å for Cu and 1.301 Å for Cl. The α values used in the atomic region were those determined by Schwarz.[19] The calculation was considered converged when the largest relative change in the potential between subsequent iterations was less than 0.001; the spin-restricted ground state of the D_{4h} ion converged after 49 iterations, while that of the D_{2d} ion reached convergence after 35 iterations. Most of the calculations were performed at MIT on a Honeywell Level 68/DPS computer, with an approximate average CPU time of 1 min/iteration for the spin-restricted calculations.

All ultraviolet photoelectron spectra (UPS) were obtained with He(II) (40.8 eV) radiation in an ion-pumped ultrahigh vacuum (UHV) system equipped with a Physical Electronics (PHI) double-pass cylindrical mirror analyzer (CMA) with integral electron gun, a differentially pumped windowless He dc discharge source, and a variable-temperature sample manipulator, as previously described.[20] A PHI Mg Kα (1253.6 eV) X-ray source was employed for acquisition of core-level spectra.

Both Cu^{2+} salts studied were found to reduce readily during exposure to high-energy electron beams (i.e., Auger) or Ar ion bombardment, and therefore neither of these standard surface science techniques was useful in characterization of the $CuCl_4^{2-}$ surfaces. Extended X-ray irradiation also caused reduction of the Cu^{2+}, and therefore all XPS measurements were performed at half power (10 KV, 20 mA) and at ~100 K. The Cu^{2+} reduction was monitored by following the disappearance of the characteristic Cu^{2+} satellites, which appear ~10 eV to higher binding energy than the $2p_{3/2,1/2}$ core levels (931 and 951 eV) and which are not observed in the Cu(0) and Cu(I) spectra.[21] Clean surfaces (as determined by XPS) were obtained by the mechanical "polishing" of single-crystal samples [$(CH_3NH_3)_2CuCl_4$ ~10 × 10 × 1.5 mm³, Cs_2CuCl_4 ~6 × 5 × 3 mm³] in vacuo by using a ceramic file of our own design, which was mounted on a rotary motion feed through. The use of single-crystal samples ensured that removal of contaminated or reduced surface layers via this filing technique exposed clean $CuCl_4^{2-}$ surfaces for further study.

Due to the insulating nature of these salts, surface charging is a significant problem, and therefore all He(II) UPS spectra were taken at room temperature with the aid of a low-energy defocused flood of electrons from the CMA integral electron gun. Charging makes the determination of absolute binding energies difficult, and therefore all $CuCl_4^{2-}$ spectra are referenced to features in their respective counterion UPS spectra.

Results and Interpretation

(A) Assignment of D_{4h} $CuCl_4^{2-}$. In the square planar limit (see Figure 1), the 12 Cl 3p valence orbitals split into three sets of equivalent orbitals, p(π) in-plane, p(π) out-of-plane, and p(σ). In D_{4h} geometry, each set further splits into three symmetry-defined molecular orbitals. Of the nine possible charge-transfer transitions, three are electric dipole allowed; those from the e_u levels are x,y polarized and that from the b_{2u} level is z polarized.

The low-temperature (7 K) optical absorption spectra of the charge-transfer region of the three square-planar monomers $(metH)_2CuCl_4$, $(N\text{-mpH})_2CuCl_4$, and $(creat)_2CuCl_4$ and of the

(13) McGinnety, J. A. *J. Am. Chem. Soc.* **1972**, *94*, 8406.
(14) Wilson, R. B.; Solomon, E. I. *Inorg. Chem.* **1978**, *17*, 1729.
(15) Anex, B. G. *Mol. Cryst.* **1966**, *1*, 1.
(16) (a) Hans, A.; Waylonis, J. E. *J. Opt. Soc. Am.* **1961**, *51*, 719. (b) Bennet, H. E.; Silver, M.; Ashley, E. J. *Ibid.* **1963**, *53*, 1089.
(17) Kronig, R. de L. *J. Opt. Soc. Am.* **1926**, *12*, 547.
(18) (a) Slater, J. C. *Adv. Quantum Chem.* **1972**, *6*, 1. (b) Slater, J. C. "Quantum Theory of Molecules and Solids"; McGraw-Hill: New York, 1974; Vol. 4. (c) Johnson, K. H.; Norman, J. G., Jr.; Connolly, J. W. D. In "Computational Methods for Large Molecules and Localized States in Solids"; Herman, F., McLean, A. D., Nesbet, R. K., Eds.; Plenum Press: New York, 1973; p 161. (d) Johnson, K. H. *Adv. Quantum Chem.* **1973**, *7*, 143.
(19) Schwarz, K. *Phys. Rev. B* **1972**, *5*, 2466.
(20) Gay, R. R.; Nodine, M. H.; Solomon, E. I.; Henrich, V. E.; Zeiger, H. J. *J. Am. Chem. Soc.* **1980**, *102*, 6752.
(21) (a) Frost, D. C.; Ishitani, A.; McDowell, C. A. *Mol. Phys.* **1972**, *24*, 861. (b) Hufner, S. *Top. Appl. Phys.* **1979**, *27*, 177.

Table I. Peak Maxima of $CuCl_4^{2-}$ (D_{4h}) from Polarized Single-Crystal Optical Absorption and Reflectance Spectroscopy[a]

$CuCl_4^{2-}$ salt	peak maxima (cm^{-1})			
	A	B	C	D
$(creat)_2CuCl_4$	22 800 (A)	24 600 (A)	27 800 (R) (~x)	37 300 (R) (~x)
			26 500 (R) (~y)	38 900 (R) (~y)
$(metH)_2CuCl_4$	20 300 (A)	22 400 (A)	26 700 (A) (~z)	
$(C_2H_5NH_3)_2CuCl_4$		23 700 (A)	26 400 (R)	35 700 (R)
		23 000 (R)		
$(N\text{-}mpH)_2CuCl_4$		23 700 (A)	26 400 (R) (~x)	37 400 (R) (~x)
		22 900 (R)	25 700 (R) (~y)	38 000 (R) (~y)

[a] A = absorption data; R = reflectance data.

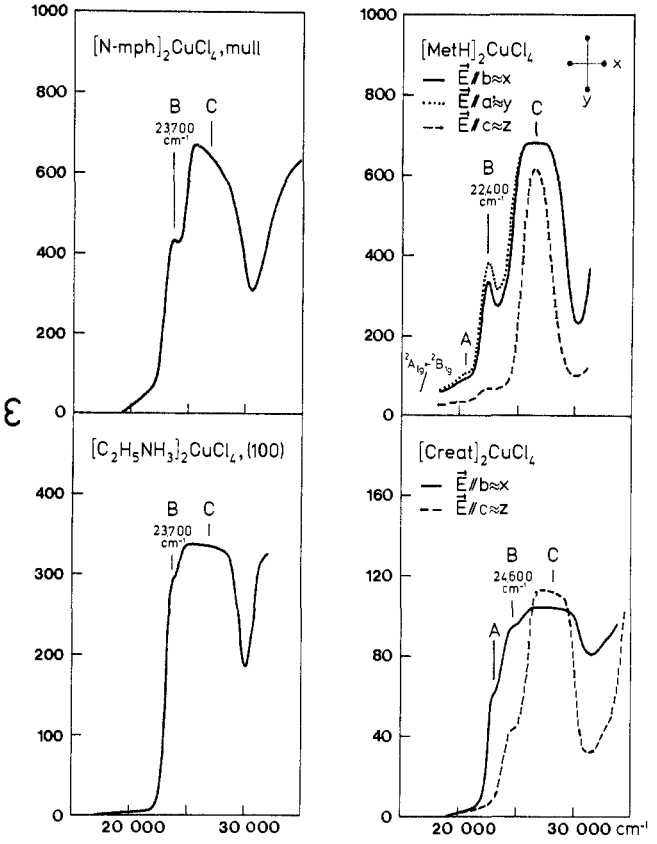

Figure 2. Low-temperature (7 K) absorption spectra of the three square-planar monomers and of the tetragonal monomer $(C_2H_5NH_3)_2CuCl_4$. The spectrum of $[N\text{-}mpH]_2CuCl_4$ was taken with the sample as a mull; the spectra of the other three salts are of single crystals. See text for explanation of band shapes.

tetragonal monomer $(C_2H_5NH_3)_2CuCl_4$ are shown in Figure 2. The spectrum of $(N\text{-}mpH)_2CuCl_4$ is that of a Nujol mull; the three others are single-crystal spectra, typically taken on crystals 15–60 μm thick. Values of peak maxima are presented in Table I. In almost all cases, the top of the most intense band (which is labeled C) is distorted; this is because at high absorbances the amount of stray light is comparable to the amount of light transmitted through the sample.

The charge-transfer spectrum of the tetragonal monomer is very similar to that of $(N\text{-}mpH)_2CuCl_4$. This is to be expected since in the tetragonal monomer the $Cu-Cl_{ax}$ bonds are much longer than the $Cu-Cl_{eq}$ bonds, and the axial chlorides are equatorial ligands to the adjacent copper atoms in the two-dimensional structure. As seen in the Experimental Section (eq 3–8), the crystal axes in $(metH)_2CuCl_4$ and $(creat)_2CuCl_4$ correlate extremely well with the molecular axes defined by the D_{2h} symmetry of the $CuCl_4^{2-}$ ion. Hence, for both of these salts, bands A–C of the absorption spectra are all x,y polarized.

The particularly low crystalline concentration of $(metH)_2CuCl_4$ (1.63 M) has made it possible to observe the undistorted shape of band C with the incident light polarized along the c axis of the crystal. The temperature dependence of this band is shown in

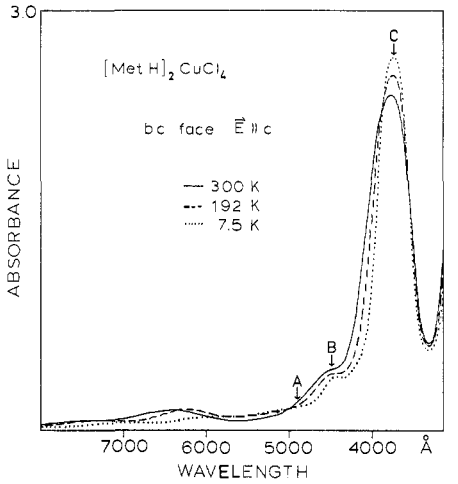

Figure 3. Temperature dependence of band C taken with $\vec{E}$ parallel to c on the {100} face of bis(methadonium) tetrachlorocuprate(II).

Figure 3. As the temperature is decreased, band C becomes sharper, keeping its total integrated intensity constant. This indicates that band C is an allowed transition. Thus, since band C is x,y polarized and allowed, it must be a transition originating from an e_u orbital. Unfortunately, overlap of the bands does not allow one to conclude anything about the temperature dependences of bands A and B.

Specular reflectance spectroscopy was used to probe bands B and C further and to extend our spectral studies to higher energy. Figure 4 shows the room-temperature single-crystal reflectance data for $(N\text{-}mpH)_2CuCl_4$, $(creat)_2CuCl_4$, and $(C_2H_5NH_3)_2CuCl_4$ after a Kramers–Kronig transformation was performed. Bands B and C are again observed; in addition, a new, intense band, which we label D, is found at ~10 000 cm^{-1} above band C (see Table I). The spectrum taken approximately along the z molecular axis (i.e., parallel to c on the {100} face) of $(creat)_2CuCl_4$ is devoid of any features, even in the region of band D. Hence, like all of the other transitions, band D is x,y polarized. Furthermore, both bands C and D are at somewhat different energies in the x and y polarizations. This is consistent with the splitting of a degenerate excited state by the D_{2h} distortion of the $CuCl_4^{2-}$ ion. Thus, bands C and D are both assigned as the electric dipole allowed $^2E_u \leftarrow {}^2B_{1g}$ ($4e_u(\pi) \rightarrow 3b_{1g}$ and $3e_u(\sigma) \rightarrow 3b_{1g}$) transitions. In addition, the absence of any z-polarized transitions with significant intensity in the spectrum of $(creat)_2CuCl_4$, even at low temperature, is of interest since one $^2B_{2u} \leftarrow {}^2B_{1g}$ ($1b_{2u}(\pi) \rightarrow 3b_{1g}$) transition from the out-of-plane Cl $p(\pi)$ orbitals is group theoretically allowed (see Figure 1). Finally, bands C and D in the $(creat)_2CuCl_4$ are blue-shifted relative to those of $(N\text{-}mpH)_2CuCl_4$ and have a larger low-symmetry splitting. This is consistent with $(creat)_2CuCl_4$ having the shortest average Cu–Cl bond length (2.251 Å; this will raise the half-filled $d_{x^2-y^2}$ orbital) and the largest D_{2h} distortion (0.035 Å) of all the square-planar salts (see Experimental Section).

Given these assignments of bands C and D, bands A and B may be assigned through a reexamination of the absorption spectra of Figure 2. In $(metH)_2CuCl_4$, the intensity of band A is comparable to that of the highest energy d–d band ($^2A_{1g} \leftarrow {}^2B_{1g}$; $a_{1g}(z^2) \rightarrow b_{1g}$).[22] In the same salt, band A also exhibits an interesting

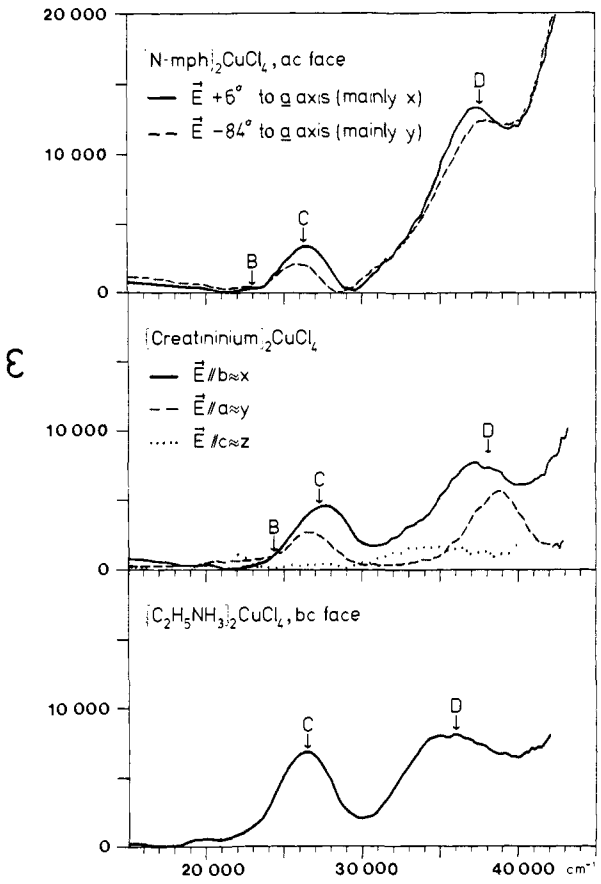

Figure 4. Kramers–Kronig transformed room-temperature single-crystal reflectance spectra of the square-planar monomers $[N\text{-mpH}]_2CuCl_4$ and $[creat]_2CuCl_4$ and of the tetragonal monomer $(C_2H_5NH_3)_2CuCl_4$.

low-symmetry splitting of $\sim$125 cm^{-1} in the polarized spectra taken on the *a'b* face. Nevertheless, because band A is not present in all salts (see, for example, the spectra of $(N\text{-mpH})_2CuCl_4$ and $(C_2H_5NH_3)_2CuCl_4$ in Figure 2) and because of some variability in its intensity relative to other bands when crystals of different batches are used, we have attributed band A to an impurity.[23] As seen in Figure 2, band B is not low-symmetry split in *x* and *y* polarization. In addition, like bands C and D, it is blue shifted in $(creat)_2CuCl_4$ compared to $(N\text{-mpH})_2CuCl_4$. This can again be correlated with the shorter average Cu–Cl bond length in $(creat)_2CuCl_4$. On the other hand, band B is at lower energy in $(metH)_2CuCl_4$ than in $(N\text{-mpH})_2CuCl_4$, even though the bands C of both salts occur at roughly the same energy and they have virtually the same average Cu–Cl bond length (2.268 vs. 2.265 Å). Since $(metH)_2CuCl_4$ differs from $(N\text{-mpH})_2CuCl_4$, $(creat)_2CuCl_4$, and $(C_2H_5NH_3)_2CuCl_4$ only by its lack of inplane ("bifurcated") hydrogen bonding, one would expect band B to originate from an orbital that can be affected by in-plane perturbations. Therefore, band B, the lowest energy charge-transfer transition, must be a transition from an in-plane, nondegenerate molecular orbital composed of Cl p(π) orbitals. Both an a_{2g} and a b_{2g} orbital fit these criteria. However, the $1a_{2g}$ level is nonbonding and is therefore expected to be at much lower binding energy than the strongly bonding $1b_{2g}$ orbital. Thus, band B is assigned as $^2A_{2g} \leftarrow {}^2B_{1g}$ ($1a_{2g}(nb) \rightarrow 3b_{1g}$), consistent with our X$\alpha$ calculations (vide infra). The *x,y* polarization of this transition indicates that it gains its intensity through mixing of the $^2A_{2g}$ excited state with ^2E_u excited states via e_u molecular vibrations.

(22) Desjardins, S. R., unpublished results.

(23) At the moment, it appears reasonable to associate band A to a ligand-field transition of the impurity $CuCl_3OH^{2-}$, with the low symmetry of this ion being responsible for the large intensity of the transition. The observed band shape supports this hypothesis, being very similar in full width at half maximum to the bandshape of the ligand-field bands of $(N\text{-mpH})_2CuCl_4$ as reported by Hitchman and Cassidy.[4d]

Table II. Correlations of Experimentally Observed and SCF-Xα-SW Calculated Transition Energies for the D_{4h} and D_{2d} $CuCl_4^{2-}$

all possible CT trans	calcd trans energy, cm^{-1}	exptl obsd trans energy, cm^{-1}	trans[a] energy differences: calcd	trans[a] energy differences: obsd
D_{4h} $CuCl_4^{2-}$ [b]				
$^2A_{2g} \leftarrow {}^2B_{1g}$ ($1a_{2g}(nb) \rightarrow 3b_{1g}$)	16 870	23 700[d]	0	0
$^2E_u \leftarrow {}^2B_{1g}$ ($4e_u(\pi) \rightarrow 3b_{1g}$)	20 430	26 400[e]	3 650	2 700
$^2B_{2u} \leftarrow {}^2B_{1g}$ ($1b_{2u}(\pi) \rightarrow 3b_{1g}$)	21 550			
$^2A_{2u} \leftarrow {}^2B_{1g}$ ($2a_{2u}(\pi) \rightarrow 3b_{1g}$)	26 960			
$^2E_g \leftarrow {}^2B_{1g}$ ($1e_g(\pi) \rightarrow 3b_{1g}$)	28 130			
$^2E_u \leftarrow {}^2B_{1g}$ ($3e_u(\sigma) \rightarrow 3b_{1g}$)	30 010	35 900[e]	13 140	12 220
$^2B_{2g} \leftarrow {}^2B_{1g}$ ($1b_{2g}(\pi) \rightarrow 3b_{1g}$)	31 450			
$^2B_{1g} \leftarrow {}^2B_{1g}$ ($2b_{1g}(\sigma) \rightarrow 3b_{1g}$)	34 880			
$^2A_{1g} \leftarrow {}^2B_{1g}$ ($2a_{1g}(\sigma) \rightarrow 3b_{1g}$)	39 570			
D_{2d} $CuCl_4^{2-}$ [c]				
$^2A_2 \leftarrow {}^2B_2$ ($1a_2(nb) \rightarrow 5b_2$)	15 440	22 700	0	0
$^2E \leftarrow {}^2B_2$ ($5e(\pi) \rightarrow 5b_2$)	16 360	24 730	920	2 030
$^2A_1 \leftarrow {}^2B_2$ ($3a_1(\pi) \rightarrow 5b_2$)	21 620			
$^2B_2 \leftarrow {}^2B_2$ ($4b_2(\pi) \rightarrow 5b_2$)	21 790			
$^2E \leftarrow {}^2B_2$ ($4e(\pi) \rightarrow 5b_2$)	22 680	28 880	7 240	6 180
$^2B_1 \leftarrow {}^2B_2$ ($1b_1(\pi) \rightarrow 5b_2$)	25 040			
$^2E \leftarrow {}^2B_2$ ($3e(\sigma) \rightarrow 5b_2$)	26 710	33 480	11 270	10 780
$^2B_2 \leftarrow {}^2B_2$ ($3b_2(\sigma) \rightarrow 5b_2$)	29 430			
$^2A_1 \leftarrow {}^2B_2$ ($2a_1(\sigma) \rightarrow 5b_2$)	33 790	43 000	18 350	20 300

[a] The transition-energy differences are all tabulated with respect to the lowest energy charge-transfer transitions [$^2A_{2g} \leftarrow {}^2B_{1g}$ ($1a_{1g}(nb) \rightarrow 3b_{1g}$) in D_{4h} and $^2A_2 \leftarrow {}^2B_2$ ($1a_2(nb) \rightarrow 5b_2$) in D_{2d}]. [b] Unpolarized spectra from $(C_2H_5NH_3)_2CuCl_4$. [c] Average of *x*-, *y*-, and *z*-polarized transition energies from Cs_2CuCl_4.[3c] [d] Absorption data. [e] Reflectance data.

The results of our SCF-Xα-SW calculations on the D_{4h} $CuCl_4^{2-}$ ion are presented in Figure 5 (ground-state orbital energies) and in Table II and Figure 10 (transition-state energies). These calculations are in qualitative agreement with the SCF-Xα-SW ground-state calculation of Zerner et al.[5l] on the square-planar $(N\text{-mpH})_2CuCl_4$ salt, the SCF-Xα-SW calculation of Johnson et al.[5j] on the tetragonal $(NH_4)_2CuCl_4$ salt, and the ab initio calculation of Demuynck et al.[5k] In our Xα calculation, the d–d transition manifold is found to overlap the charge-transfer manifold, in disagreement with definitive spectral assignments that place the highest energy d–d transition 6000–8000 cm^{-1} lower in energy than the lowest energy charge-transfer transition.[4d] In fact, the calculated ground-state Xα molecular orbital ordering would suggest that the charge-transfer transition ($^2A_{2g} \leftarrow {}^2B_{1g}$; $1a_{2g}(nb) \rightarrow 3b_{1g}$) is lower in energy than any of the d–d transitions. However, the transition-state Xα calculations are in better agreement with experiment, predicting this charge-transfer transition to be higher in energy than two of the three d–d transitions. In addition, the calculated order of the d–d transitions ($^2E_g \leq {}^2B_{2g} < {}^2A_{1g} \leftarrow {}^2B_{1g}$) deviates somewhat from the experimental assignment ($^2B_{2g} < {}^2E_g < {}^2A_{1g} \leftarrow {}^2B_{1g}$).[4d] These inconsistencies are probably artifacts of the scattered wave formalism, in which the potential in the intersphere region (the region within the outer "Watson" sphere but outside of the atomic spheres) is assumed to be constant. For $CuCl_4^{2-}$ in the D_{4h} geometry, the volume of this region is relatively large, introducing some errors in the calculation.[24] In contrast, in the D_{2d} geometry the volume of the intersphere region is much less, and a clear separation of the d–d and charge-transfer manifolds, as well as the proper d orbital ordering, is calculated (vide infra).

While the absolute energies of the charge-transfer transitions are calculated to be $\sim$7000 cm^{-1} lower than observed, the ordering and separation of the calculated charge-transfer transition energies (in D_{4h}) correlate well with our assignment of the spectrum (see Table II). The lowest energy charge-transfer transition was calculated to be from the $1a_{2g}$ in-plane nonbonding orbital to the $d_{x^2-y^2}$ orbital ($^2A_{2g} \leftarrow {}^2B_{1g}$). This is the only charge-transfer

(24) Johnson, K. H., personal communication.

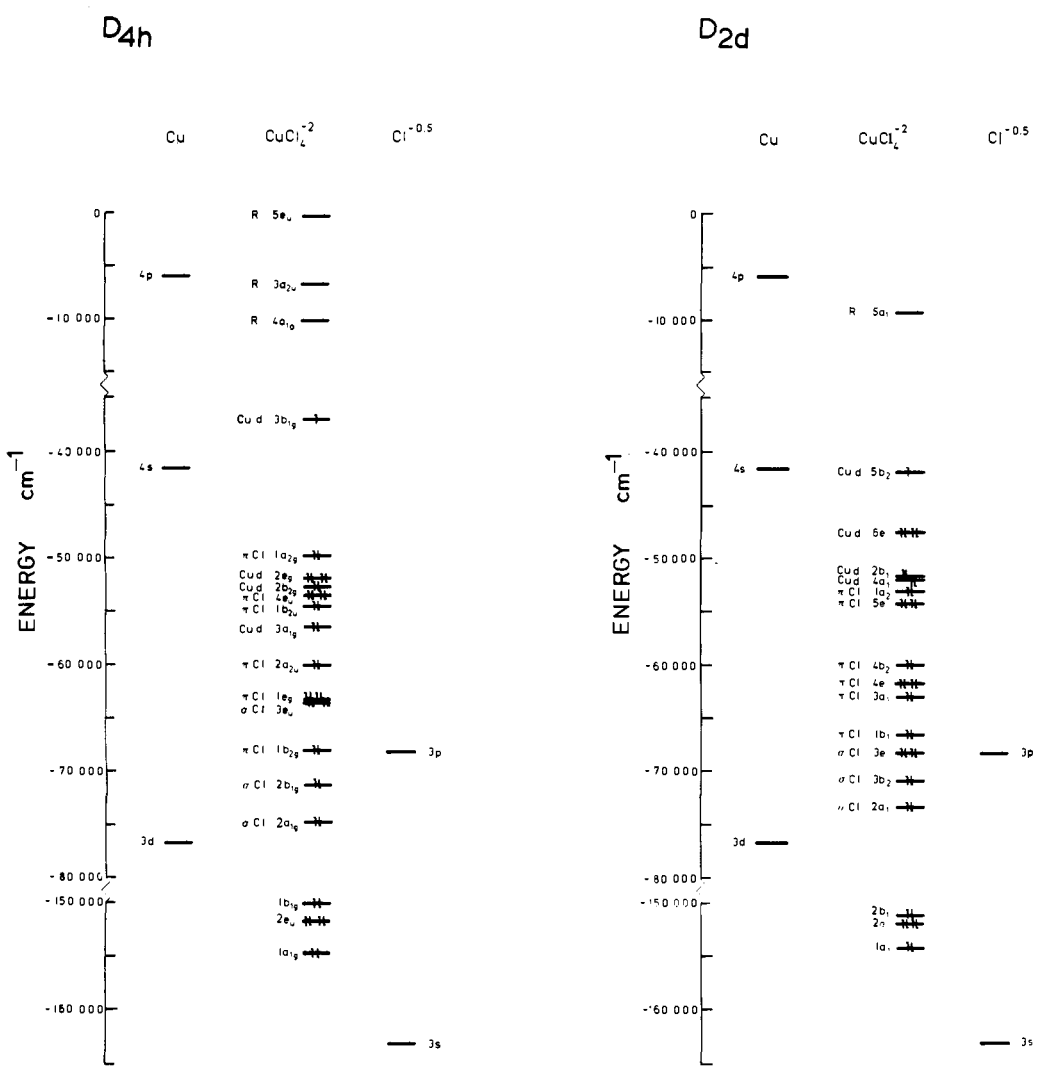

Figure 5. Ground-state molecular orbital diagrams for the upper valence region of $CuCl_4^{2-}$, as determined by SCF-Xα-SW calculations. Predominant characters of the molecular orbitals are indicated. P denotes unoccupied Rydberg-like orbitals. In addition, the energies of the Cu and $Cl^{-0.5}$ upper valence orbitals are given.

transition calculated to have a lower energy than the charge-transfer transition from the $4e_u(\pi)$ orbital; the calculated separation between these two transitions is $\sim$3600 cm^{-1}. The transition from the $3e_u(\sigma)$ orbital is predicted to lie $\sim$10 000 cm^{-1} higher in energy than the $4e_u(\pi) \rightarrow 3b_{1g}$ transition. The close correlation of the relative energies of these three transitions with our absorption and reflectance data (see Table II) confirms the assignment of band B as a $^2A_{2g} \leftarrow {}^2B_{1g}$ ($1a_{2g}$(nb) $\rightarrow 3b_{1g}$) transition, band C as a $^2E_u \leftarrow {}^2B_{1g}$ ($4e_u(\pi) \rightarrow 3b_{1g}$) transition, and band D as a $^2E_u \leftarrow {}^2B_{1g}$ ($3e_u(\sigma) \rightarrow 3b_{1g}$) transition. The possibility that band D might be associated with the $^2E_u \leftarrow {}^2B_{1g}$ ($3b_{1g} \rightarrow 5e_u$) Rydberg transition is rejected on energetic grounds. Finally, the group theoretically allowed (z polarized) $^2B_{2u} \leftarrow {}^2B_{1g}$ ($1b_{2u}(\pi) \rightarrow 3b_{1g}$) transition is calculated to be 4700 cm^{-1} above the $^2A_{2g} \leftarrow {}^2B_{1g}$ ($1a_{2g}(\pi) \rightarrow 3b_{1g}$) transition; this allowed transition is neither observed experimentally nor predicted to have any intensity (vide infra).

(B) Correlation to D_{2d} $CuCl_4^{2-}$. We can now consider the D_{2d} $CuCl_4^{2-}$ qualitative molecular orbital energy level diagram (see Figure 1). In T_d geometry, the 12 Cl 3p valence orbitals divide into five molecular orbitals, which split further in D_{2d} geometry into six p(π) and three p(σ) molecular orbitals. Of the nine possible charge-transfer transitions, those from the e molecular orbitals are x,y polarized while those from the a_1 molecular orbitals are z polarized. Hence, five electric dipole allowed transitions are expected. Many spectroscopic and theoretical studies have been performed on the D_{2d} $CuCl_4^{2-}$ ion[3,5a,b,d,e,g-i,k-m] in an attempt to assign bands 1–5 of the absorption spectrum shown in Figure 6. The presently accepted assignment[3g] attributes the entire

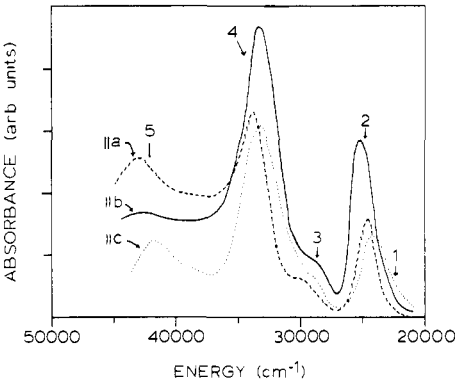

Figure 6. Polarized single-crystal absorption spectra of copper(II)-doped Cs_2ZnCl_4. Spectra with $\vec{E}$ parallel to a and $\vec{E}$ parallel to b taken at liquid-air temperatures with light incident on the {001} face. Spectrum with $\vec{E}$ parallel to c obtained at room temperature with light incident on the {100} face and scaled such that the band at 24 600 cm^{-1} is 20% higher for $\vec{E}$ parallel to a than for $\vec{E}$ parallel to c, as suggested in ref 3c. Relative orientations of molecular and crystal axes are as follows: y parallel to b, x and z are in the ac plane, with z 50° off of a and 40° off of c. Adapted from ref 3c.

UV–vis charge-transfer spectrum to transitions from the p(π) molecular orbitals of the Cl ligands. The specific assignment of the spectrum is as follows: band 1, $^2A_2(^2T_1$,nb) $\leftarrow {}^2B_2$ ($1a_2$(nb) $\rightarrow 5b_2$); band 2, $^2E(^2T_1$,nb) $\leftarrow {}^2B_2$ ($5e(\pi) \rightarrow 5b_2$); band 3, $^2B_2$ ($^2T_2,\pi$) $\leftarrow {}^2B_2$ ($4b_2(\pi) \rightarrow 5b_2$); band 4, $^2E(^2T_2,\pi) \leftarrow {}^2B_2$ ($4e(\pi)$

$\rightarrow 5b_2$); band 5, $^2A_1$ ($^2E,\pi$) $\leftarrow$ $^2B_2$ ($3a_1(\pi) \rightarrow 5b_2$), where the tetrahedral parentages of the excited states are indicated in the parentheses (see Figure 1). This assignment was derived from the combined results of optical absorption and magnetic circular dichroism experiments. The polarized single-crystal optical studies of the Cs_2CuCl_4 salt[3b,c] clearly show bands 2 and 4 to be x,y polarized and split, indicating that they are due to transitions to ^2E excited states (in D_{2d}), while band 5 is z polarized and therefore must be a $^2A_1 \leftarrow {}^2B_2$ ($a_1 \rightarrow 5b_2$) transition. The variable-temperature MCD study[3g] demonstrates that the spectrum is dominated by C terms that result from spin–orbit coupling in the D_{2d} double group. A moment analysis of the MCD spectrum of the region, including bands 1 and 2, very strongly supports the assignment of these bands to excited states derived from a $^2T_1$ (nb) parent state. The first moment provides the spin–orbit splitting of the excited state, which in this region increases by a factor of 4 on going from the $CuCl_4^{2-}$ ion to the $CuBr_4^{2-}$ ion. This change correlates well with the ratio of the spin–orbit coupling constants of the two halogens, which are 590 cm^{-1} for Cl^- and 2460 cm^{-1} for Br^-. This close correlation demonstrates that the transitions producing bands 1 and 2 originate from orbitals that are predominantly ligand in character and therefore likely derived from the nonbonding t_1 orbital. The assignment of bands 3–5 to transitions originating from π orbitals is less clear because of the possible overlap with other charge-transfer transitions, complicating both the resolution of the MCD into specific C terms and a quantitative moment analysis.

Correlation of the D_{4h} $CuCl_4^{2-}$ assignment of section A to the D_{2d} spectrum (see Figures 4 and 6) demonstrates that reassignment of bands 4 and 5 is required; these bands are likely due to σ, and not π, charge-transfer transitions. The present assignment of the D_{2d} charge-transfer spectrum, which attributes all of the UV–vis features to transitions from π ligand orbitals, would require the $^2E(^2T_2,\sigma) \leftarrow {}^2B_2$ ($3e(\sigma) \rightarrow 5b_2$) transition to be at very high energy beyond the UV spectral region. However, since the $d_{x^2-y^2}$ orbital will be stabilized upon distortion from D_{4h} to D_{2d}, the simplest approximation (see Introduction) predicts that the charge-transfer transition involving the $3e_u$ (σ) orbital (band D in the D_{4h} site) should be higher in energy than the transition from the $3e(t_2,\sigma)$ orbital in D_{2d}. Hence, the D_{4h} results indicate that band 4 is the $^2E(^2T_2,\sigma) \leftarrow {}^2B_2$ ($3e(\sigma) \rightarrow 5b_2$) transition and therefore that band 5 should be associated with the highest energy charge-transfer transition, $^2A_1(^2A_1,\sigma) \leftarrow {}^2B_2$ ($2a_1(\sigma) \rightarrow 5b_2$). Finally, the moderate intensity and x,y polarization of band 3 (Figure 6) suggest that it is probably the remaining x,y-allowed $^2E(^2T_2,\pi) \leftarrow {}^2B_2$ ($4e(\pi) \rightarrow 5b_2$) transition.

This assignment of the D_{2d} $CuCl_4^{2-}$ spectrum is strongly supported by our Xα calculations. The results of these calculations for the D_{2d} $CuCl_4^{2-}$ are given in Figure 5 (ground-state energies) and in Table II and Figure 10 (transition-state energies). It should be noted that the d–d manifold is calculated to be separate from and lower in energy than the manifold of charge-transfer states, consistent with experimental results. In addition, the order of the d–d transitions is in agreement with polarized spectral assignments. These improvements over the calculated results for the D_{4h} site are probably due to the smaller volume of the intersphere region (region of constant potential) in the D_{2d} geometry. While the calculated energies of the charge-transfer transitions are again clearly too low (by $\sim$7000 cm^{-1}, see Table II), the differences in the calculated energies are in extremely good agreement with our assignment of the D_{2d} charge-transfer spectrum. In addition, the differences between the calculated energies of corresponding transitions in the D_{4h} and D_{2d} sites agree well with the shifts of these transitions as determined experimentally, lending further support to our assignment of the D_{2d} spectrum (see Discussion). Furthermore, the results of single-crystal ultraviolet photoelectron spectroscopic studies of Cs_2CuCl_4, $(C_2H_5NH_3)_2CuCl_4$, and $(CH_3NH_3)_2CuCl_4$ also support our conclusion that the UV–vis charge-transfer spectrum of the D_{2d} $CuCl_4^{2-}$ complex contains both the Cl p(π) and Cl p(σ) charge-transfer transitions (vide infra).

Using this assignment for the D_{4h} and D_{2d} charge-transfer spectra, we may now examine the mechanisms that give these transitions their intensity[25] and determine the reasons for the absence of the group theoretically allowed $^2B_{2u} \leftarrow {}^2B_{1g}$ ($1b_{2u}(\pi) \rightarrow 3b_{1g}$) and $^2A_1 \leftarrow {}^2B_2$ ($3a_1(\pi) \rightarrow 5b_2$) transitions in the D_{4h} and D_{2d} spectra. In these studies, only the contributions from the ligand 3p orbitals in the ground and excited states have been considered; this approximation has been demonstrated by van der Avoird and Ros[25a] to provide reasonable values for oscillator strengths. In this method, the wave function of a molecular orbital is written as

$$\psi = C_1\Phi_M + C_2\chi_L$$

where Φ_M = atomic orbital of the central ion and

$$\chi_L = \sum_{\alpha=1}^{4} \sum_{ml=-1}^{1} C_{\alpha_{ml}}\Phi_{\alpha_{ml}}$$

with $\Phi_{\alpha_{ml}}$ = atomic orbital of ligand α with the specified m_l values, and C_1 and C_2 are normalization constants.

In the calculation of the oscillator strengths, only integrals over orbitals on the same ligand are considered, and the radial part of the 3p wave function, which is a function of energy, is assumed to be invariant over the small energy range of the transition. Thus the dipole moment integrals have the following form:

$$D = \langle\Phi'|\vec{r}|\Phi\rangle \approx C'_2C_2\sum_{\alpha=1}^{4}\sum_{ml=-1}^{1} C'_{\alpha_{ml}}C_{\alpha_{ml}}\langle\Phi'_{\alpha_{ml}}|\vec{r}|\Phi_{\alpha_{ml}}\rangle \approx C'_2C_2\sum_{\alpha=1}^{4}\sum_{ml=-1}^{1} C'_{\alpha_{ml}}C_{\alpha_{ml}}\vec{r}_\alpha$$

where the prime indicates the excited state and $\vec{r}_\alpha$ is the position vector of ligand α. Oscillator strengths are then calculated through the formula

$$f_{th} = 1.085 \times 10^{11}\bar{\nu}|D|^2$$

where $\bar{\nu}$ is expressed in inverse centimeters and D in centimeters. Experimental oscillator strengths were determined through the approximation $f_{exp} \approx 4.61 \times 10^{-9}\epsilon_{max}\bar{\nu}_{1/2}$, where $\bar{\nu}_{1/2}$ is the full width at half maximum of the absorption band. The results of these calculations, using theoretical wave functions approximated from our Xα data, are shown in Table III. Although the f_{exp} values are only approximate due to the uncertainty of the base line, there is good agreement between f_{th} and f_{exp}. It is especially significant that the allowed transitions that were not observed experimentally have theoretical oscillator strengths that are several orders of magnitude less than those for the observed allowed transitions.

Table III. Oscillator Strength Calculations for Symmetry-Allowed Transitions

geometry	transition	frequency, cm^{-1} [a]	oscillator strength[b] theor	oscillator strength[b] exptl
D_{2d}[c]	$3a_1 \rightarrow 5b_2$	21 600[d]	0.0004	0.0
	$5e \rightarrow 5b_2$	24 900	0.0349	0.050
	$4e \rightarrow 5b_2$	28 400	0.0721	~0.008
	$3e \rightarrow 5b_2$	33 100	0.0941	0.095
	$2a_1 \rightarrow 5b_2$	43 000	0.199	0.03
D_{4h}[e]	$1b_{2u} \rightarrow 3b_{1g}$	21 600[d]	0.0	0.0
	$4e_u \rightarrow 3b_{1g}$	26 400	0.104	0.055
	$3e_u \rightarrow 3b_{1g}$	37 400	0.355	0.405

[a] For transitions from e or e_u orbitals, the frequency of the x-polarized transition is given. [b] For transitions from e or e_u orbitals, only the x-polarized component of both the theoretical and experimental oscillator strength is given. [c] Experimental data of Cs_2CuCl_4 deposited on Cs_2ZnCl_4 crystal.[3c] [d] Value from Xα transition-state calculations. [e] Experimental data from spectrum of $(NmpH)_2CuCl_4$.

(25) (a) van der Avoird, A.; Ros, P. *Theor. Chim. Acta* **1966**, *4*, 13. (b) Ros, P.; Van der Avoird, A.; Schuit, G. C. A. *Coord. Chem. Rev.* **1967**, *2*, 77. (c) Wolfsberg, M.; Helmholz, L. *J. Chem. Phys.* **1952**, *20*, 837. (d) Ballhausen, C. J.; Liehr, A. D. *J. Mol. Spectrosc.* **1958**, *2*, 342. (e) Ballhausen, C. J.; Liehr, A. D. *Ibid.* **1960**, *4*, 190. (f) Carrington, A.; Schonland, D. S. *Mol. Phys.* **1960**, *3*, 331. (g) Wiers, B. H.; Reynolds, W. L. *Inorg. Chem.* **1966**, *5*, 2016. (h) Vanquickenborne, L. G.; Verdonck, E. *Ibid.* **1976**, *15*, 454. (i) Poole, R. T.; Jenkin, J. G.; Liesegang, J.; Leckey, R. C. G. *Phys. Rev. B* **1975**, *11*, 5179.

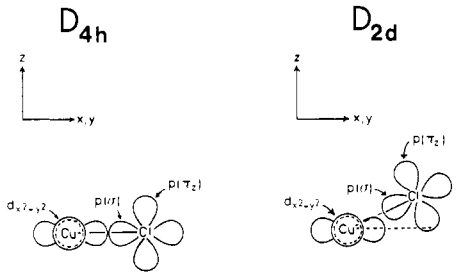

Figure 7. Orientation of the Cl p(σ) and p(π_z) orbitals relative to the Cu $d_{x^2-y^2}$ orbital and the molecular z axis in the D_{4h} and D_{2d} geometries.

In D_{4h}, the $3b_{1g}$ orbital has contributions only from the Cl p(σ) orbitals (see Figure 1). Since in this model the intensity is derived from overlap of the ligand 3p orbitals in the ground and excited states, it is therefore the ligand p(σ) character (see Figure 7) in the orbital from which the excited electron originates that determines the intensities of the charge-transfer transitions. The $3e_u$ level has ~70% p(σ) character, making the $^2E_u \leftarrow {}^2B_{1g}$ ($3e_u(\sigma) \rightarrow 3b_{1g}$) transition quite intense, while the $^2E_u \leftarrow {}^2B_{1g}$ ($4e_u(\pi) \rightarrow 3b_{1g}$) transition gains intensity by configurational mixing of p(σ) character from the $3e_u$ level. Since the $1b_{2u}$ orbital contains no Cl p(σ) character, it has no overlap with the $3b_{1g}$ ligand orbitals and thus the $^2B_{2u} \leftarrow {}^2B_{1g}$ ($1b_{2u}(\pi) \rightarrow 3b_{1g}$) transition has no intensity even though it is group theoretically allowed.

In the D_{2d} geometry, the amounts and phases of both σ and π_z Cl p character in the excited states are important, since the $5b_2$ orbital has contributions from both of these types of ligand orbitals (see Figure 7). The agreement between the observed and theoretical oscillator strengths for the $^2E \leftarrow {}^2B_2$ ($5e(\pi) \rightarrow 5b_2$) transition and the $^2E \leftarrow {}^2B_2$ ($3e(\sigma) \rightarrow 5b_2$) transition is quite good. Although an accurate value of the experimental oscillator strength of the $^2E \leftarrow {}^2B_2$ ($4e(\pi) \rightarrow 5b_2$) transition is difficult to determine because of the overlap of bands 3 and 4, it is clear that f_{th} for this transition is too high. This may be due to an overestimation in the Xα results of the p(σ) character in the 4e orbital; if this p(σ) contribution is reduced, f_{th} decreases significantly to a limiting value of 0.0097 at zero 4e–3e mixing. Most important is the result that f_{th} for the $^2A_1 \leftarrow {}^2B_2$ ($3a_1(\pi) \rightarrow 5b_2$) transition is smaller than the f_{th} values for the other allowed transitions by over 2 orders of magnitude. This is consistent with the present assignment of the D_{2d} charge-transfer spectrum, which proposes that this transition is not observed.

Finally, it has been noted that the d–d bands of the square-planar salts have little intensity in the z polarization.[4d] Our polarized single-crystal studies of the charge-transfer spectrum show that there are no low-lying charge-transfer states with intensity in the z direction. Therefore, the lack of z polarization in the d–d bands appears to be due to the absence of z-polarized charge-transfer states at an energy low enough for effective vibronic mixing into the d–d transitions.

(C) UPS Results for D_{2d} and D_{4h} $CuCl_4^{2-}$: Correlation with Optical Results. As an additional probe of the electronic structure of the $CuCl_4^{2-}$ valence band, ultraviolet photoelectron spectroscopic (UPS) studies utilizing He(II) radiation have been performed on both the distorted tetrahedral (D_{2d}) Cs_2CuCl_4 and the tetragonal (D_{4h}) $(C_2H_5NH_3)_2CuCl_4$ and $(CH_3NH_3)_2CuCl_4$ tetrachlorocuprates. The application of UPS to studies of the valence electronic structure of gas-phase (or sublimed) organometallic and inorganic complexes,[26] solid-state semiconductors, metals, and some insulators,[27] has been well established. However, there is a significant lack of literature pertaining to UPS studies on nonvolatile solid ionic coordination complexes. This must be partly attributed to the complications of sample preparation (these complexes will not sublime or withstand elevated temperatures, are unstable to Ar ion bombardment, and are often too small to cleave) as well as sample charging, which tends to broaden the spectra and make referencing difficult. However, the UPS spectra of several $CuCl_4^{2-}$ coordination complexes are shown here to provide information complementary to that obtained from detailed optical absorption studies, specifically regarding the assignment of the D_{2d} $CuCl_4^{2-}$ charge-transfer spectrum.

Table IV. $CuCl_4^{2-}$ Transition-State Ionization Calculation

D_{2d}	ionization energy, eV	D_{4h}	ionization energy, eV
$5b_2$	7.96	$3b_{1g}$	7.41
6e	8.63	$1a_{2g}$(nb)	8.71
$4a_1$	9.10	$2e_g$	9.12
$1a_2$(nb)	9.12	$3a_{1g}$	9.12
$2b_1$	9.20	$4e_u(\pi)$	9.15
$5e(\pi)$	9.24	$1b_{2u}(\pi)$	9.25
$4b_2(\pi)$	9.89	$2b_{2g}$	9.45
$4e(\pi)$	10.13	$2a_{2u}(\pi)$	9.89
$3a_1(\pi)$	11.07	$3e_u(\sigma)$	10.40
$2a_1(\sigma)$	11.70	$1b_{2g}(\pi)$	11.78
$1b_1(\pi)$	11.75	$1e_g(\pi)$	11.86
$3e(\sigma)$	11.88	$2a_{1g}(\sigma)$	11.98
$3b_2(\sigma)$	12.16	$2b_{1g}(\sigma)$	12.29
$2b_2$	21.40	$1b_{1g}$	21.28
2e	21.49	$2e_u$	21.46
$1a_1$	21.75	$1a_{1g}$	21.83

Table V. $1a_2$(nb)–$2a_1(\sigma)$ Splitting in D_{2d} $CuCl_4^{2-}$

method		energy, eV
Xα	ground state	2.5
	transition-state optical	2.3
	transition-state UPS	2.6
UPS	$CuCl_4^{2-}$	2.1 ± 0.3
	$TiCl_4$	1.8
optical	(1) this assignment (43 000-cm^{-1} band = $2a_1(\sigma)$)	2.5
	(2) previous assignment (43 000-cm^{-1} band = $2a_1(\pi)$ + transition-state Xα $3a_1(\pi)$–$2a_1(\sigma)$ = 1.5)	4.0

In Figure 8a are shown the He(II) UPS of Cs_2CuCl_4(s) along with comparative spectra of CsCl(s) (adapted from ref 28) and $TiCl_4$(g) (adapted from ref 29). Since charging of the Cs_2CuCl_4 makes it difficult to determine absolute binding energies, the CsCl has been used as a reference by aligning the Cs^+ 5p photoemission features (binding energy (BE) = 15.85 eV) of CsCl with those of Cs_2CuCl_4. Composite peaks A and B in the Cs_2CuCl_4 spectrum (separated by 1.4 eV, fwhm ~3.8 eV) are attributed to photoemission from the $CuCl_4^{2-}$ unit. The nonbonding Cl 3p ionizations of CsCl (BE = 9.15 eV) fall under region A of the Cs_2CuCl_4 spectrum.

The related tetrahedral molecules[31] $TiCl_4$ (d^0) and VCl_4 (d^1)

(26) (a) Furlani, C.; Cauletti, C. *Struct. Bonding (Berlin)* **1978**, *35*, 119. (b) Cowley, A. H. *Prog. Inorg. Chem.* **1979**, *26*, 45. (c) Hillier, I. H. *Pure Appl. Chem.* **1979**, *51*, 2183. (d) Bancroft, G. M.; Sham, T. K.; Eastman, D. E.; Gudat, W. *J. Am. Chem. Soc.* **1977**, *99*, 1752. (e) Orchard, A. F. In "Electronic States of Inorganic Compounds: New Experimental Techniques"; NATO Advanced Study Institute Series, Day, P., Ed.; Reidel: Boston, 1975; p 339. (f) Considine, M.; Connor, J. A.; Hillier, I. H. *Inorg. Chem.* **1977**, *16*, 1392. (g) Connor, J. A.; Considine, M.; Hillier, I. H. *J. Chem. Soc., Faraday Trans. 2* **1978**, *74*, 1285. (h) Connor, J. A.; Considine, M.; Hillier, I. H.; Briggs, D. *J. Electron. Spectrosc. Relat. Phenom.* **1977**, *12*, 143. (i) Poole, R. T.; Jenkin, J. G.; Liesegang, J.; Leckey, R. C. G. *Phys. Rev. B* **1975**, *11*, 5179.

(27) (a) Ley, L.; Cardona, M., Eds. "Topics in Applied Physics: Photoemission in Solids I"; Springer-Verlag: New York, 1979; Vol. 26. (b) Ley, L.; Cardona, M., Eds. "Topics in Applied Physics: Photoemissions in Solids II"; Springer-Verlag: New York, 1979, Vol. 27. (c) Lindau, I.; Spicer, W. E. In "Synchrotron Radiation Research"; Winick, H., Doniach, S., Eds.; Plenum Press: New York, 1980; p 159. (d) Goldman, A.; Tejeda, J.; Shevchik, N. J.; Cardona, M. *Phys. Rev. B* **1974**, *10*, 4388. (e) Ishii, T.; Kono, S.; Suzuki, S.; Nagakira, I.; Sagawa, T.; Kato, R.; Watanabe, M.; Sato, S. *Ibid.* **1975**, *12*, 4320. (f) Eastman, D. E.; Freeouf, J. L. *Phys. Rev. Lett.* **1975**, *34*, 395. (g) Grobman, W. D.; Koch, E. E. In ref 27b, Chapter 5 and references therein.

(28) Poole, R. T.; Jenkin, J. G.; Leckey, R. C. G.; Liesegang, J. *Chem. Phys. Lett.* **1973**, *22*, 101.

(29) Egdell, R. G.; Orchard, A. F.; Lloyd, R. D.; Richardson, N. V. *J. Electron Spectrosc. Relat. Phenom.* **1977**, *12*, 415.

(30) Rabalais, J. W. "Principles of Ultraviolet Photoelectron Spectroscopy"; Wiley: New York, 1977; Chapter 5.

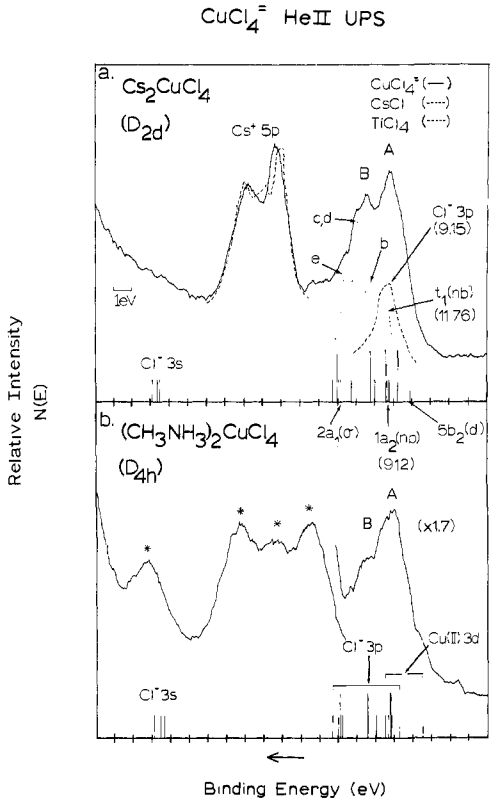

Figure 8. He(II) ultraviolet photoemission spectra (UPS) of (a) Cs_2CuCl_4 and (b) $(CH_3NH_3)_2CuCl_4$. Results of the corresponding SCF-Xα-SW transition-state ionization calculations are superimposed below each spectrum. In (a), the spectra of single-crystal Cs_2CuCl_4 and CsCl(s) (adapted from ref 28) have been aligned at the Cs^+ 5p features. The $TiCl_4$(g) (adapted from ref 29) and the Xα results are aligned such that the $TiCl_4$(g) t_1(nb) ionization (11.76 eV), the CsCl Cl 3p ionization (9.15 eV), and the Xα a_2(nb) level (9.12 eV) coincide. The $TiCl_4$ UPS spectrum is scaled such that the total integrated intensity of the CsCl Cl 3p feature is approximately equal to half of the total integrated intensity of the four chlorides in $TiCl_4$. The other $TiCl_4$ features labeled *b*–*e* are assigned to the $t_2(\pi)$, $e(\pi)$, $a_1(\sigma)$, and $t_2(\sigma)$ ionizations, respectively.[32c] The D_{4h} and D_{2d} $CuCl_4^{2-}$ spectra are aligned by matching positions of the ionizations labeled A; the Xα results in the two geometries are aligned at the calculated Cl 3s level, although the Cl 3s ionization is not experimentally observed, due to its low photoionization cross section at this energy.[27d] A and B in both spectra indicate features due to the $CuCl_4^{2-}$ species, while $CH_3NH_3^+$ counterion features are marked by an asterisk. Relative intensities in the Xα ionization calculations are approximated by the fractional parentage method[30] for an open-shell, nondegenerate ground-state configuration; the effects of multiplet splitting have not been taken into account.[35]

(not shown) are also particularly useful for comparison to the d^9 $CuCl_4^{2-}$, since their photoelectron spectra (obtained in the gas phase and thus without complications due to charging) have been extensively studied.[29,31e,32] It is generally agreed that the $TiCl_4$ ionizations at 11.76 and 12.77 eV (in Figure 8a) originate in the t_1(nb) and $t_2(\pi)$ Cl molecular orbitals, respectively (see Figure 1). The assignment of peaks c, d, and e at binding energies of ~13.2, ~13.5, and 13.96 eV has recently been revised. Peaks c and d were originally assigned to the $1e(\pi)$ and $2t_2(\sigma)$ ionizations, and peak e to the $2a_1(\sigma)$ ionization (in agreement with ab initio calculations[31e]). However, a more recent study[32c] of the theoretical and experimental photoionization cross sections of the $TiCl_4$ UPS has given support for the reassignment of these peaks to the $2e(\pi) < 2a_1(\sigma) < 2t_2(\sigma)$ ionizations, respectively, also in agreement with an Xα transition-state ionization potential calculation.[31f] The $TiCl_4$ He(II) UPS spectrum has been aligned in Figure 8a such that the t_1(nb) photoemission coincides with that from the nb Cl 3p in CsCl. This places the bonding Cl features in $TiCl_4$ under the region of peak B in Cs_2CuCl_4, which is therefore assigned to predominantly Cl 3p ionizations.

Our D_{2d} transition-state ionization Xα calculation (see Table V) is also superimposed beneath the three UPS spectra in Figure 8a by aligning the calculated a_2(nb) (t_1(nb) in T_d symmetry; 9.12 eV) with the experimentally observed nb Cl levels of CsCl and $TiCl_4$. The Xα ionization potential calculation predicts ionization of the Cu 3d and Cl 3p orbitals to occur over the ranges 7.96–9.20 eV (d manifold width of 1.24 eV) and 9.12–12.16 eV (Cl manifold width of 3.04 eV), respectively. The experimental widths of the Cu 3d and Cl 3p manifolds (as approximated from the fwhm of the two overlapping features A and B) are 1.6 ± 0.3 and 2.5 ± 0.3 eV. Thus, comparison of the calculation and the UPS spectrum further suggests that peak A can be attributed to predominantly Cu 3d and peak B to Cl 3p ionizations. This is also in agreement with the UPS spectra of $TiCl_4$(g) and VCl_4(g), where the Cl 3p manifold of states are observed to be 2.2 and 2.5 eV wide.

In a correlation of the UPS and optical spectra, it is important to account for the effects of many-electron reorganization (due to changes in electron–electron repulsion and orbital relaxation), since this can cause the energy of a charge-transfer transition to be significantly different than the experimental binding energy difference between two UPS features (vide infra). These effects will be largest when the orbitals involved have quite different localization and bonding properties and hence different reorganization energies. Therefore, in correlating to optical spectra, the differences in energies of transitions from orbitals with similar localization properties will provide the most accurate comparison; in the D_{2d} $CuCl_4^{2-}$, the $1a_2$(nb) and $2a_1(\sigma)$ molecular orbitals would be expected to have the same reorganization trends (vide infra). This expectation is based on the results of our ground state,

Table VI. Xα Ground-State Charge Density

level	% contributions Cu	Cl	int	out	Cu angular contributions		
				D_{2d}			
$5b_2$	43	47	6	4	4% P	95% D	
$6e$	44	46	7	3	5% P	95% D	
$2b_1$	50	38	10	2	100% D		
$4a_1$	41	47	10	2	1% S	99% D	
$1a_2$	0	83	14	2			
$5e$	1	81	15	2			
$4b_2$	4	72	22	2			
$4e$	9	69	20	2			
$3a_1$	52	35	12	1	3% S	96% D	
$1b_1$	47	39	13	1	100% D		
$3e$	51	44	3	2	5% P	95% D	
$3b_2$	56	41	1	2	2% P	98% D	
$2a_1$	23	65	9	3	71% S	27% D	2% F
				D_{4h}			
$3b_{1g}$	42	49	4	5	100% D		
$1a_{2g}$	0	86	12	2			
$2e_g$	40	48	10	2	100% D		
$2b_{2g}$	60	31	8	1	100% D		
$4e_u$	2	82	12	4			
$1b_{2u}$	0	82	15	2			
$3a_{1g}$	85	6	8	0	6% S	94% D	
$2a_{2u}$	2	74	23	2			
$1e_g$	57	32	11	1	100% D		
$3e_u$	7	78	12	4			
$1b_{2g}$	38	46	15	1	100% D		
$2b_{1g}$	58	40	1	2	100% D		
$2a_{1g}$	28	62	7	3	48% S	52% D	

(31) (a) $TiCl_4$ and VCl_4 are both T_d ($\beta = 54.7°$) with M–Cl bond lengths of 2.14 Å[31b] and 2.17 Å,[31c] respectively, while Cs_2CuCl_4 is D_{2d} ($\beta \approx 65°$) with a Cu–Cl bond length of 2.23 Å.[12] Ground-state calculations predict the width of the Cl 3p manifold to be 1.9,[31d] 2.3,[31e] and ~2.0 eV,[31f] in $TiCl_4$, 2.1 eV,[31d] in VCl_4, and 2.5 eV (this work) in $CuCl^{2-}$. (b) Alderdice, D. S. *J. Mol. Spectrosc.* **1965**, *15*, 509. (c) Spiridonov, V. P.; Ramanov, G. V. *Zh. Strukt. Khim.* **1967**, *3*, 160. (d) Paramesewaran, T.; Ellis, D. E. *J. Chem. Phys.* **1973**, *58*, 2088. (e) Hillier, I. H.; Kendrick, J. *Inorg. Chem.* **1976**, *15*, 520. (f) Tossell, J. A. *Chem. Phys. Lett.* **1979**, *65*, 371.

(32) (a) Green, J. C.; Green, L. M. H.; Joachim, P. J.; Orchard, A. F.; Turner, D. W. *Philos. Trans. R. Soc. London, Ser. A* **1970**, *268*, 111. (b) Cox, P. A.; Evans, S.; Hamnett, A.; Orchard, A. F. *Chem. Phys. Lett.* **1970**, *7*, 414. (c) Bancroft, G. M.; Pellach, E.; Tse, J. S. *Inorg. Chem.* **1982**, *21*, 2950.

transition-state optical, and transition-state ionization potential calculations (see Table VI), where the $1a_2(nb) \leftrightarrow 2a_1(\sigma)$ splittings are 2.5, 2.3, and 2.6 eV, respectively. Consequently, the experimental $1a_2(nb) \leftrightarrow 2a_1(\sigma)$ splitting can be directly compared between UPS and optical methods. That is, even if the absolute reorganization energies for the UPS and optical excitations are significantly different, the observed splitting between these states should remain approximately constant. The assignment of the D_{2d} $CuCl_4^{2-}$ UPS spectrum has provided a value for the width of the total Cl 3p manifold of 2.5 ± 0.3 eV. Although (due to overlap), the $1a_2(nb) \leftrightarrow 2a_1(\sigma)$ splitting cannot be determined directly from the UPS spectrum, it is expected to be ~0.4 eV less than the total Cl manifold width (as predicted by the $CuCl_4^{2-}$ transition-state ionization calculation; Table IV)[33] and will thus be 2.1 ± 0.3 eV. This is compared to the high-resolution UPS of $TiCl_4$, which has a $t_1(nb) \leftrightarrow a_1(\sigma)$ splitting of 1.8 eV.

This value for the $1a_2(nb) \leftrightarrow 2a_1(\sigma)$ splitting is in good agreement with the present assignment of the Cs_2CuCl_4 (D_{2d}) optical charge-transfer spectrum where the observed splitting between the $^2A_2 \leftarrow {}^2B_2$ ($1a_2(nb) \rightarrow 5b_2$) (22 700 cm^{-1}) and the $^2A_1 \leftarrow {}^2B_2$ ($2a_1(\sigma) \rightarrow 5b_2$) (43 000 cm^{-1}) is equal to 2.5 eV. Alternatively, if the prior assignment of the D_{2d} absorption spectrum is used, the charge-transfer band at 43 000 cm^{-1} would be attributed to the $^2A_1 \leftarrow {}^2B_2$ ($3a_1(\pi) \rightarrow 5b_2$) transition and hence the $^2A_1 \leftarrow {}^2B_2$ ($2a_1(\sigma) \rightarrow 5b_2$) transition would be expected to fall 1.5 eV to higher energy (as predicted by the transition-state optical calculation; Table II), giving a $1a_2(nb) \leftrightarrow 2a_1(\sigma)$ splitting of 4.0 eV. As shown in Table VI, this is significantly higher than that experimentally observed in the $TiCl_4$ or $CuCl_4^{2-}$ UPS spectra or that calculated by the Xα transition-state method. Further, with a $1a_2(nb) \leftrightarrow 2a_1(\sigma)$ splitting of ~4.0 eV (and a $2a_1(\sigma) \leftrightarrow 3b_2(\sigma)$ splitting of ~0.4 eV) and a Cu 3d manifold splitting of 1.6 eV, the total $CuCl_4^{2-}$ valence band width would be estimated to be 5.5–6.0 eV wide. This would require the UPS of the D_{2d} $CuCl_4^{2-}$ to be at least 1.5 eV wider than that which is experimentally observed. [The UPS of $TiCl_4$ (and VCl_4) would also be expected to show valence band widths much larger than that observed in Figure 8a.] Thus, an assignment of the D_{2d} charge-transfer spectrum consistent with the UPS requires the band at 43 000 cm^{-1} to be due to the $^2A_1 \leftarrow {}^2B_2$ ($2a_1(\sigma) \rightarrow 5b_2$) charge-transfer transition.

Finally, He(II) UPS of the tetragonal $(C_2H_5NH_3)_2CuCl_4$ and $(CH_3NH_3)_2CuCl_4$ tetrachlorocuprate salts have also been obtained. A representative spectrum of $(CH_3NH_3)_2CuCl_4$ is shown in Figure 8b with the transition-state ionization potential Xα calculation (see Table V) superimposed. Features A and B are again attributed to the $CuCl_4^{2-}$ unit while the remaining features are due to the ($CH_3NH_3^+$) counterion. Comparison to the D_{2d} UPS spectrum shows that the spectrum of the D_{4h} unit is quite similar. Overlap of the counterion features makes exact determination of the valence band width difficult; however, via comparison to the D_{2d} UPS spectrum and the D_{4h} ionization potential calculation, peak A is assigned to predominantly Cu 3d and peak B to predominantly Cl 3p photoionization. The approximate width of the $CuCl_4^{2-}$ valence band its again consistent with the D_{4h} optical charge-transfer spectrum.

Having obtained both experimental and theoretical values for the UPS and optical transition energies, we can now quantitatively correlate between these techniques in order to evaluate the relative contributions of many-electron reorganization[34] (due to changes in electron–electron repulsion and orbital relaxation) to the UPS and optical spectra. The results of the Xα transition-state optical and ionization potential calculations are correlated in Figure 9 by aligning the ground state of the molecule [$^2B_2(5b_2)$] with the ground state of the molecular ion [$^1A_1(5b_2)$]. It should be immediately noted that there are large changes in magnitude of the energy splitting of the various molecular and ionic excited states when comparing between the two different spectroscopic techniques. This is quite contrary to that expected in an independent particle frozen orbital approximation, where a quantitative one to one correspondence would be predicted between the relative energies of excited states within the molecule and within the molecular ion. These deviations are due to changes in electron–electron repulsion that occur in response to removal or transferral of electron density during the excitation process. That these two transition-state calculations (and the related UPS and optical data) yield excited-state splittings that are quite different indicates that the effects of many-electron reorganization must be considered in any correlation of UPS and optical data.

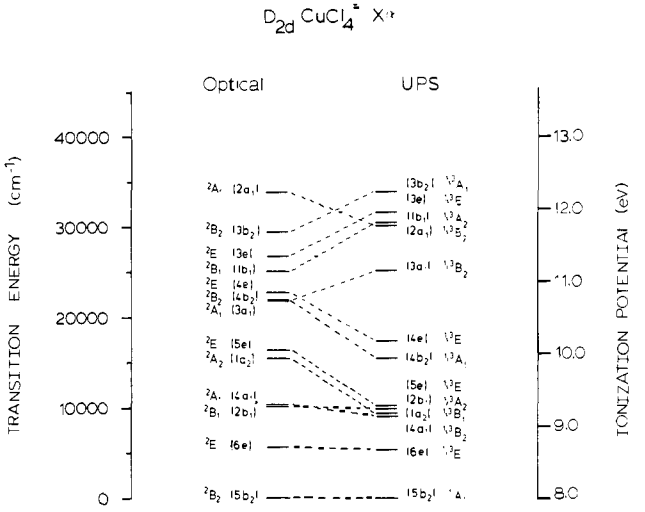

Figure 9. Correlation of Xα transition-state optical absorption and ionization potential calculations for $CuCl_4^{2-}$ in D_{2d} geometry. The calculations have been aligned such that the ground state of the molecule $^2B_2$ ($5b_2$) coincides with the ground state of the molecular ion $^1A_1$ ($5b_2$). The possibility of photoionization to singlet and triplet final states is indicated.[36]

In photoelectron spectroscopy, changes in electron–electron repulsion and orbital relaxation stabilize the ionized state relative to an independent particle frozen state and lead to a reduction in the binding energy of all UPS features. The magnitude of the valence orbital reorganization energy is dependent upon the localization properties of the electron being ionized; a final state hole in a smaller, more localized molecular orbital will induce a greater reduction in electron–electron repulsion upon ionization than a delocalized hole state. Similarly, in optical absorption, the magnitudes of transition energies (relative to an independent particle frozen orbital picture) are dependent upon the localization properties of the two orbitals involved in the electron transfer. For example, excitation of an electron from a delocalized to a highly localized orbital will cause significant increase in electron–electron repulsion; this destabilizes the excited state and causes an increase in the transition energy. On the other hand, excitation of an electron between orbitals with similar localization properties will cause little change in electron–electron repulsion, and thus the transition energy will be close to that predicted by an independent particle.

Therefore, when correlating UPS and optical spectra, the differences in energies of states with similar localization properties and hence similar reorganization energies will remain constant and can be compared; i.e., even though the absolute magnitude of many-electron reorganization may be quite different within the molecule and the molecular ion, the splittings of molecular and ionic states with comparable reorganization energies will remain

(33) This is further supported by the $TiCl_4$ Xα calculation[31f] and UPS,[32c] which suggest that the $a_1(\sigma)$ ionization is at ~0.5 eV lower binding energy than the $t_2(\sigma)$ ionization.

(34) (a) Shirley, D. A. In ref 27a, Chapter 4 and references therein. (b) Hüfner, S. In ref 27b, Chapter 3 and references therein. (c) Case, D. A.; Cook, M.; Karplus, M. *J. Chem. Phys.* **1980**, *73*, 3294. (d) Lamson, S. H.; Messmer, R. P. *Phys. Rev. B* **1982**, *25*, 7209. (e) Evans, S.; Guest, M. F.; Hillier, I. H.; Orchard, A. F. *J. Chem. Soc., Faraday Trans. 2*, **1974**, *70*, 417. (f) Ferreira, R. *Struct. Bonding (Berlin)* **1976**, *31*, 1.

(35) Although multiplet splitting will produce 25 possible final states (depicted in Figure 9), the single–triplet energy splittings have not been calculated. Sample charging, however, prevents resolution of this multiplet structure.

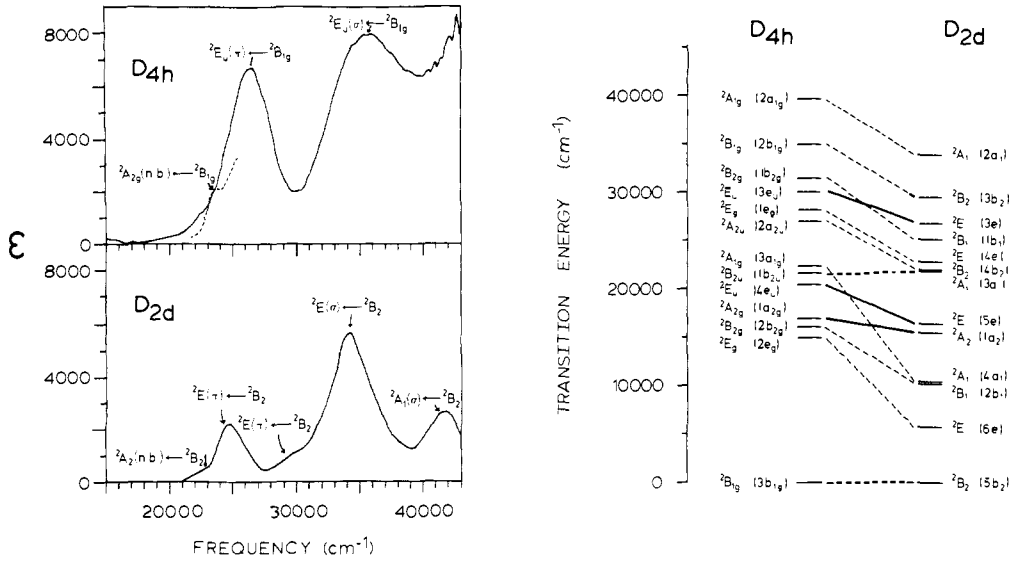

Figure 10. Experimental and theoretical comparisons of $CuCl_4^{2-}$ charge-transfer features in D_{4h} and D_{2d} geometries. Left: Single-crystal room-temperature reflectance (—) and low-temperature polarized absorption (---) spectra of D_{4h} $CuCl_4^{2-}$ (upper) and low-temperature absorption spectrum of a D_{2d} $CuCl_4^{2-}$ film (adapted from ref 3g; lower). Spectral assignments presented in this paper are indicated. Right: Energies of ligand-field and charge-transfer transitions in the D_{4h} and D_{2d} geometries as determined through transition-state SCF-Xα-SW calculations. Correlations between states in the two geometries are indicated by solid lines in the case of excited states observed in the D_{4h} spectrum and dashed lines for all other states.

Table VII. Correlation of the Charge-Transfer Energy Shifts upon Distortion of $CuCl_4^{2-}$ from D_{4h} to D_{2d}

related charge-transfer trans		theor Xα trans energy shift, cm^{-1}	exptl obsd trans energy shift, cm^{-1} [a]
D_{4h}	D_{2d}		
$^2A_{2g} \leftarrow {}^2B_{1g}$ ($1a_{2g} \rightarrow 3b_{1g}$)	$^2A_2 \leftarrow {}^2B_2$ ($1a_2 \rightarrow 5b_2$)	−1430	−1000
$^2E_u \leftarrow {}^2B_{1g}$ ($4e_u \rightarrow 3b_{1g}$)	$^2E \leftarrow {}^2B_2$ ($5e \rightarrow 5b_2$)	−4070	−1670
$^2E_u \leftarrow {}^2B_{1g}$ ($3e_u \rightarrow 3b_{1g}$)	$^2E \leftarrow {}^2B_2$ ($3e \rightarrow 5b_2$)	−3300	−2420

[a] Experimental values from $(C_2H_5NH_3)_2CuCl_4$ (D_{4h}) absorption and reflectance spectra and Cs_2CuCl_4 (D_{2d}) absorption spectra (see Table III).

the same, and this splitting will be close to that predicted in an independent particle analysis. Alternatively, it can be misleading to compare the UPS and optical splittings for two states with different localization properties since differential many-electron repulsion can significantly change their relative energies.

A closer look at Figure 9 indicates that the states arising from d–d transitions and d orbital ionizations are at approximately the same energy relative to the molecular and ionic ground states. Since the 6e, $4a_1$, and $2b_1$ d orbitals have similar atomic character and localization properties (see Table VII) as the ground-state $5b_2$ d orbital, changes in electron–electron repulsion and orbital relaxation are not expected to strongly affect these energy splittings. The observed UPS and optical d manifold of states will thus be similar in magnitude.

The picture is more complex for the charge-transfer transitions. The predominantly nonbonding Cl molecular orbitals (those orbitals [$1a_2$(nb), 5e, $4b_2$, 4e] that our calculation predicts to have little overlap with the Cu 3d orbitals; see Table VII) are strongly delocalized on the four Cl ligands. The charge-transfer transitions from these orbitals to the $5b_2$ $d_{x^2-y^2}$ orbital (localized on the metal) are significantly shifted (~0.8 eV) to higher energy relative to the corresponding UPS ionizations. On the other hand, the charge-transfer transitions from those Cl orbitals strongly involved in bonding to the metal 3d orbitals ($3b_2$, 3e, $1b_1$, $3a_1$) are shifted to ~0.5 eV lower energy than the corresponding UPS ionizations. In the case of the $2a_1$, there is significant metal–ligand overlap. However, this is with the metal 4s orbital (which is more diffuse and still results in a delocalized electron density). Therefore, its reorganization trends are qualitatively similar to the non-bonding orbitals. In Figure 9, it is seen that the energy splitting between states can change by as much as 1.5 eV (i.e., $3a_1(\pi) \leftrightarrow 4b_2(\pi)$ splitting) in correlating from UPS to optical spectra. From our previous discussion, this derives from differences in localization (bonding) properties of the orbitals involved in the excitation, which result in differences in electron–electron repulsion.

The experimental correlation of the D_{2d} $CuCl_4^{2-}$ charge-transfer spectrum with the high-resolution UPS of $TiCl_4$(g)[32c] gives strong supporting evidence for the existence of these differences in many-electron effects. In the D_{2d} charge-transfer spectrum, the $^2A_1 \leftarrow {}^2B_2$ ($2a_1(\sigma) \rightarrow 5b_2$) is the highest energy charge-transfer transition, whereas in the $TiCl_4$ UPS, the $2a_1(\sigma)$ ionization falls ~0.4 eV to lower binding energy than the $2t_2(\sigma)$ ionization. Thus the reversal in ordering of these excited states predicted in Figure 9 by the theoretical Xα results is verified experimentally.

Discussion

Having obtained a consistent assignment of the charge-transfer spectrum of $CuCl_4^{2-}$ in the D_{4h} and D_{2d} chlorocuprates, we can now examine the shifts in energies of the dominant transitions as the geometry changes from the square planar (D_{4h}) to the distorted tetrahedral (D_{2d}) limit. The experimental and theoretical results of this correlation are presented in Figure 10. In the simplest approximation, one might expect the energies of all the Cl 3p → Cu $3d_{x^2-y^2}$ charge-transfer transitions to parallel the shift in energies of the $d_{x^2-y^2}$ orbital. The distortion from D_{4h} to D_{2d} lowers the crystal-field repulsion of an electron in this orbital and thus shifts it to deeper binding energy. Both a ligand-field calculation[5f] [$W(b_2[d_{x^2-y^2}]) = 12(3\cos^2\beta - 1)Ds - 0.5(35\sin^4\beta + \delta)Dt$, where $\delta = 35\cos^4\beta - 30\cos^2\beta + 3$, $Ds = ze\langle r^2\rangle/21a^3 = 415$ cm^{-1}, $Dt = ze\langle r^4\rangle/21a^5 = 345$ cm^{-1}, $\beta = 65°$ in D_{2d} $CuCl_4^{2-}$, and $\beta = 90°$ in D_{4h} $CuCl_4^{2-}$] and the SCF-Xα-SW calculation presented here predict a stabilization of $d_{x^2-y^2}$ by ~5000 cm^{-1}. This in turn would predict a decrease in energy of all the charge-transfer transitions by this same amount.

The experimental and theoretical shifts for the $^2A_{2g}$(nb), $^2E_u(\pi)$, and $^2E_u(\sigma) \leftarrow {}^2B_{1g}$ ($1a_{2g}$, $4e_u$ and $3e_u \rightarrow 3b_{1g}$) [in D_{4h}] transitions are given in Table VII and Figure 10. Clearly these three transitions are observed to shift in energy by differing amounts and all are observed to decrease by significantly less than the 5000 cm^{-1} predicted by consideration of only the $d_{x^2-y^2}$ orbital. These data give us direct experimental insight into the values of the additional factors that must contribute to the energy of charge-transfer transitions. These important contributions are expected from (1) ligand–ligand repulsion, (2) overlap-induced configuration interaction, and (3) many-electron reorganization effects.

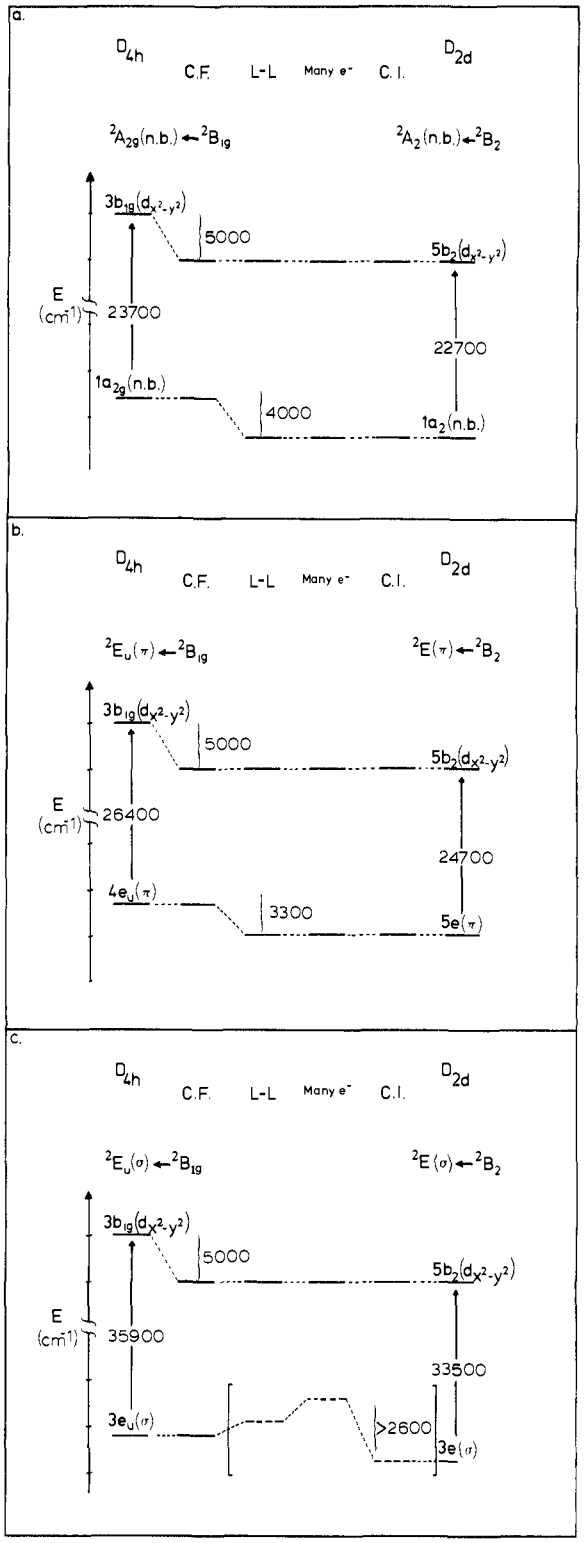

Figure 11. Factors contributing to changes in energies of the indicated transitions upon distortion of $CuCl_4^{2-}$ complex from D_{4h} to D_{2d} symmetry. Experimental transition energies are given. Abbreviations: CF, crystal field; L-L, ligand–ligand repulsion; many e⁻, many-electron (reorganization) effects; CI, configuration interaction. The experimental magnitudes of the individual effects enclosed in brackets in part c cannot be determined.

Examination of the experimental data on the $^2A_{2g} \leftarrow {}^2B_{1g}$ ($1a_{2g}(nb) \rightarrow 3b_{1g}$) transition indicates that ligand–ligand repulsion can be as significant as changes in the energy of $d_{x^2-y^2}$. The $1a_{2g}$ ($1a_2$) orbital is nonbonding in D_{4h} (and D_{2d}); hence changes in configuration interaction (which can produce changes in many-electron reorganization) are not group theoretically allowed in either geometry. The fact that this transition exhibits a negligible

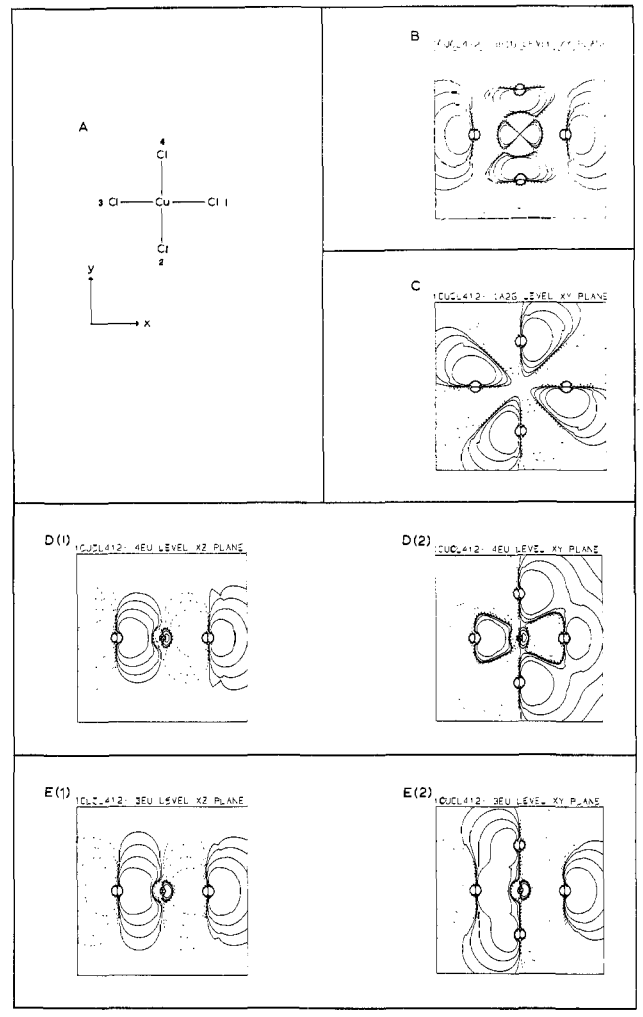

Figure 12. Electron probability density contour diagrams for selected orbitals in D_{4h} $CuCl_4^{2-}$, as determined by SCF-Xα-SW calculations. The orientations of the x and y axes relative to the $CuCl_4^{2-}$ unit are given in A, which has been drawn to the same scale as B–E.

change in energy indicates that although the $d_{x^2-y^2}$ orbital is stabilized by 5000 cm^{-1} from $D_{4h} \rightarrow D_{2d}$, there is a concurrent stabilization of the $1a_{2g}(nb)$ orbital that compensates for the effects of changes in $d_{x^2-y^2}$ (see Figure 11a). This large decrease in ligand–ligand repulsion can be visualized through the density contour diagram of the $1a_{2g}(nb)$ orbital (in D_{4h}) shown in Figure 12C, where a D_{2d} distortion raises Cl_1 and Cl_3 and lowers Cl_2 and Cl_4, thereby lowering ligand–ligand interaction between the in-plane $p(\pi)$ orbitals (i.e., Cl_1 and Cl_2).

The shifts in the e_u (D_{4h}) levels not only are influenced by changes in ligand–ligand interactions but are further complicated by changes in overlap-induced configuration interaction (CI) whereby the Cl 3p e(σ and π) are now group theoretically allowed to mix with the $e(d_{xz,yz})$ in D_{2d} symmetry. This also tends to alter the magnitude of many-electron reorganization effects that (as discussed in section C) depend strongly on the atomic character and localization properties of the orbitals.

The Xα calculation predicts that the $4e_u(\pi)$ undergoes no mixing with $d_{xz,yz}$ upon distortion to D_{2d} (see Table VI) and therefore CI will not contribute significantly to differences in transition energies. Here again, however, some decrease in ligand–ligand repulsion is expected upon distortion to D_{2d} (see contour diagram in Figure 12D), although the magnitude of this effect will be smaller than that observed for the a_{2g} orbital. (The $1a_{2g}$ has 100% $p(\pi)$ in-plane contributions and therefore greater ligand–ligand overlap than the $4e_u(\pi)$, which has contributions from in-plane σ (Cl_1 and Cl_3; 28%) and in-plane π (Cl_2 and Cl_4; 72%) character.) The 3300-cm^{-1} deviation of the transition energy from that predicted by the shift in only $d_{x^2-y^2}$ is therefore attributed to changes in ligand–ligand repulsion (see Figure 11b).

Finally, the Xα calculation (Table VI) indicates significant mixing of the $3e_u(\sigma)$ orbital with the $e(d_{xz,yz})$ upon distortion to D_{2d} (48% $d_{xz,yz}$ contribution in D_{2d} symmetry; 0% $d_{xz,yz}$ in D_{4h}). In this case, both the change in ligand–ligand interaction (see $3e_u(\sigma)$ contour diagram, Figure 12E(2)) and the change in electron–electron repulsion (due to the significant difference in d orbital character in the D_{4h} and D_{2d} geometries) are expected to decrease the energy of the $^2E_u \leftarrow {}^2B_{1g}$ ($3e_u(\sigma) \rightarrow 3b_{1g}$) transition (Figure 11c). Thus, one would expect this transition to occur at even lower energy than that predicted from consideration of only the 5000-cm^{-1} shift in $d_{x^2-y^2}$. Although experimentally this transition decreases in energy by the greatest amount, this shift is still clearly reduced from the >5000 cm^{-1} just predicted. This discrepancy must be due to the contribution of CI to the energy of the $3e_u$ level.

In summary, changes in ligand–ligand repulsion (particularly for the in-plane $p(\pi)$ orbitals) can be as important as the changes in crystal-field repulsion of the metal $d_{x^2-y^2}$ orbital in predicting the energy of charge-transfer transitions. Furthermore, for states that exhibit a significant change in ligand–metal overlap upon distortion, changes in configuration interaction and many-electron reorganization can also greatly contribute to changes in transition energies.

In addition to an examination of the factors that cause changes in charge-transfer transition energies with variations in geometry, our studies have also permitted a critical comparison of the results of SCF-Xα-SW calculations and experimental values to be made. In general, the magnitudes of the calculated transition energies are not accurate; the energies of the charge-transfer transitions are all calculated to be 65–80% of the observed energies. Also, in the D_{4h} geometry, the d–d and charge-transfer transition manifolds overlap, and the order of the d–d bands deviates from the experimental ordering. On the other hand, in the D_{2d} geometry the d–d transitions are calculated to be in the correct order and are well separated from the charge-transfer transitions. The calculated orderings of the charge-transfer transitions also agree quite well with experiment in both geometries, and the calculated and observed shifts between related transitions in the two geometries are very similar [Table VII]. Thus, while the Xα method does not always provide accurate quantitative results, it has in this case proven to be an important aid for the interpretation of charge-transfer absorption spectra.

Our studies have also allowed us to consider the sources of the intensity of charge-transfer transitions in transition-metal complexes. Through the use of our Xα results and the concept that charge-transfer transition intensity is primarily due to the overlap of ligand orbitals in the ground and excited states, the relative intensities of the charge-transfer bands of tetrachlorocuprates in both the D_{2d} and D_{4h} geometries have been explained. In the square-planar complex, the ligand 3p character in the $3b_{1g}$ orbital is completely of σ type. Therefore, the intensities of the charge-transfer transitions are determined by the amount of $3p(\sigma)$ character in the excited state. In the distorted tetrahedral site, both ligand $3p(\sigma)$ and $3p(\pi_z)$ orbitals contribute to the ground-state orbital; thus, overlap with the sum of these atomic orbitals contributes to the transition intensity. Neither the $^2B_{2u} \leftarrow {}^2B_{1g}$ ($1b_{2u}(\pi) \rightarrow 3b_{1g}$) transition (in D_{4h}) nor the $^2A_1 \leftarrow {}^2B_2$ ($3a_1(\pi) \rightarrow 5b_2$) transition (in D_{2d}) is experimentally observed in the charge-transfer spectrum. Since the $1b_{2u}$ orbital has no ligand $3p(\sigma)$ character and the relative phases of the $3p(\sigma)$ and $3p(\pi_z)$ ligand orbitals in the $3a_1$ and $5b_2$ molecular orbitals result in very little net overlap between these levels, this is to be expected.

Finally, these studies have made possible an experimental and theoretical comparison between UPS and optical spectroscopy in terms of the energy splittings of ligand molecular orbitals in the D_{2d} $CuCl_4^{2-}$ ion. It is found that a simple independent particle frozen orbital description of this correlation (i.e., a quantitative one to one correspondence between UPS and optical excited-state energies) is inappropriate, due to changes in electron–electron repulsion upon excitation. The magnitude of these many-electron reorganization effects depends strongly on the localization and bonding properties of the orbitals involved in the transition. While the relative energies of the d orbitals in optical absorption and UPS remain constant, the relative energies of the Cl to Cu charge-transfer transitions and the Cl orbital ionizations are quite different; this leads to changes in energy (by as much as 1.5 eV) and reversal in ordering of certain excited states within the Cl manifold of states when comparing between the two spectroscopic techniques. Therefore, careful consideration of many-electron reorganization is required before meaningful correlations between UPS and optical spectra can be obtained.

Acknowledgment. We gratefully acknowledge support from the National Science Foundation (E.I.S., CHE 82-04841), a Research Corp. Cottrell College Science Grant (R.L.M.), and the "Direction générale de l'enseignement supérieur" of the Province of Quebec (S.R.D.). In addition, we thank Heather Bunting for obtaining reflectance data, Dr. Harold Nelson for providing $(metH)_2CuCl_4$ crystals, Dr. Richard Harlow for unpublished crystallographic information on $(metH)_2CuCl_4$, Dean Wilcox for growing crystals of $(creat)_2CuCl_4$, and Prof. Keith Johnson and Dr. R. Scott Wallace for making their SCF-Xα-SW programs available and for assisting in the performance of the calculations. Finally, we thank Dr. Bernard Briat for useful discussions of MCD data and Francisco Leon for helpful discussions of Xα calculations.

Registry No. $(metH)_2CuCl_4$, 72268-09-8; $(N\text{-}mpH)_2CuCl_4$, 51751-77-0; $(creat)_2CuCl_4$, 85702-37-0; $(C_2H_5NH_3)_2CuCl_4$, 55940-27-7.